ESL/ TR-94/ 12-12

TWO-PHASE FLOW OF TWO HFC REFRIGERANT MIXTURES THROUGH SHORT TUBE ORIFICES

DRAFT FINAL REPORT

TASK 1

CONTRACT NO: CR-822227-01-0

PREPARED FOR THE
ENVIRONMENTAL PROTECTION AGENCY
RESEARCH TRIANGLE PARK, NC 27711

PREPARED BY:

W. Vance Payne, M.S.
Research Assistant

Dennis L. O'Neal, Ph. D., P.E.
Professor

Energy Systems Laboratory
Department of Mechanical Engineering
Texas A & M University
College Station, TX 77843

December 1994

TABLE OF CONTENTS

NOMENCLATURE

A_s	short tube cross-sectional area, in.^{2} (m^2)
C_r	oil concentration on a pure refrigerant basis
C_{tp}	correction factor for two-phase flow
D	short tube diameter, in.(mm)
D_{ref}	reference short tube diameter, 0.060 in. (1.52 mm)
DR	ratio of tube diameter to reference tube diameter, D/D_{ref}
$EVAP$	normalized downstream pressure, $(P_c-P_{down})/P_c$ (P in psia (kPa))
γ_C	dimensional gravity constant, SI unit: 1.2960×10^{10} ($s^2 \cdot N/(h^2 \cdot kN)$)
	English unit: 2.8953×10^6 ($lb_m ft^3/(lb_f in^2\ h^2)$)
L	short tube length, in. (mm)
L/D	ratio of short tube length to diameter
$\dot{m}$	mass flow rate, lb_m/h (kg/h)
m_R	mass flow ratio of oil and refrigerant mixtures to pure refrigerant
P	pressure, psia (kPa)
P_c	critical pressure, psia (kPa)
P_{down}	downstream (evaporator) pressure, psia (kPa)
P_f	adjusted downstream pressure, psia (kPa)
P_{sat}	upstream liquid saturation pressure, psia (kPa)
P_{up}	upstream (condenser) pressure, psia (kPa)
PRA	ratio of upstream pressure to critical pressure, P_{up}/P_c
Q	heat transfer rate, Btu/h (W)
$SUBC$	normalized subcooling, $(T_{sat}-T_{up})/T_c$ (T in °R (K))
T	temperature, °R (K) or °F (°C)
T_c	critical temperature, °R (K)
T_{sat}	liquid saturation temperature of the upstream fluid, °R (K)
T_{up}	temperature of upstream fluid, °R (K)
x	refrigerant quality
ρ	density, lb_m/ft^3 (kg/m^3)

CHAPTER I

INTRODUCTION

The need for new refrigerants was established when scientists first realized the ozone depleting effects of CFC and HCFC refrigerants. The chlorine atom in these refrigerants is capable of reaching the upper atmosphere where one chlorine atom can destroy more than 100,000 ozone atoms(Langley 1994). Laws have been enacted to halt the destruction of the ozone layer and force industry to find replacements for the ozone depleting refrigerants. Section 608 of the Clean Air Act (1990) prohibited the venting of ozone depleting refrigerants as of July 1, 1992. In addition the Clean Air Act (1990) also requires the EPA to develop regulations limiting the emissions of ozone depleting refrigerants. Efforts are currently underway to find CFC replacements before the complete phaseout of CFC manufacturing in January of 1996.

Much of the effort to replace CFC and HCFC refrigerants has centered on development of refrigerant mixtures that could replace R-22. Before systems can be designed with a new refrigerant (or mixture), thermodynamic and thermophysical properties must first be characterized. An important component in air conditioners is the expansion device. Because of their low cost, several manufacturers have chosen to use short tube orifices for the expansion device in their systems. Designing a system with an orifice requires knowledge of the flow characteristics of short tube orifices. Recent work on orifices has focused on R-12 and R-22 (Kim and O'Neal, 1993a; Aaron and Domanski, 1990; Krakow, 1988; and Mei, 1982). In addition, there are unpublished data on R-134a (Kim and O'Neal, 1993b) and the effect of lubricants on flow characteristics (Kim, 1993; Kim and O'Neal, 1994b).

The present study presents data for flow of two refrigerant mixtures through short tube orifices. The two mixtures were R32/125/134a (23%/25%/52% on a mass percentage basis) and R32/125 (50%/50%). The following presents results for the flow of these two refrigerants through short tube orifices of various diameters and lengths of 0.5 in (12.7 mm), 0.75 in (19.05 mm), and 1.00 in (25.4 mm) in a pure form and mixed with various mass percentages of oil.

CHAPTER II

EXPERIMENTAL SETUP

A schematic diagram of the experimental setup is shown in Figure 2.1. The test loop was designed to allow easy control of each operating parameter such as upstream subcooling or quality, upstream pressure, and downstream pressure. It also allowed for changing the oil concentration by injection of the oil into the system. The test rig consisted of three major flow loops: (1) a refrigerant flow loop containing a detachable test section, (2) a hot water flow loop used for the evaporation heat exchanger and (3) a chilled water-glycol flow loop used for the condensation heat exchanger.

A diaphragm liquid pump with a variable speed motor was used to provide a wide range of refrigerant mass flow rates. An advantage of the diaphragm pump was that it did not require lubrication as would a compressor. Thus, it allowed oil concentration to be an adjustable parameter in operating the system. The pressure entering the test section (upstream or condenser pressure) was controlled by adjusting the speed of the refrigerant pump. A hand-operated needle valve was utilized to permit precise control of upstream pressure by bypassing liquid refrigerant from the pump to the short tube exit. To provide additional flow control into the test section, a by-pass line which included a capillary tube was utilized from the pump exit to the short tube exit. The refrigerant flow rate was measured by a Coriolis effect mass flow meter in the liquid line between the pump and the evaporation heat exchanger.

The refrigerant subcooling or quality entering the test section was set by a water heated heat exchanger (evaporation heat exchanger) and a heat tape. For single-phase

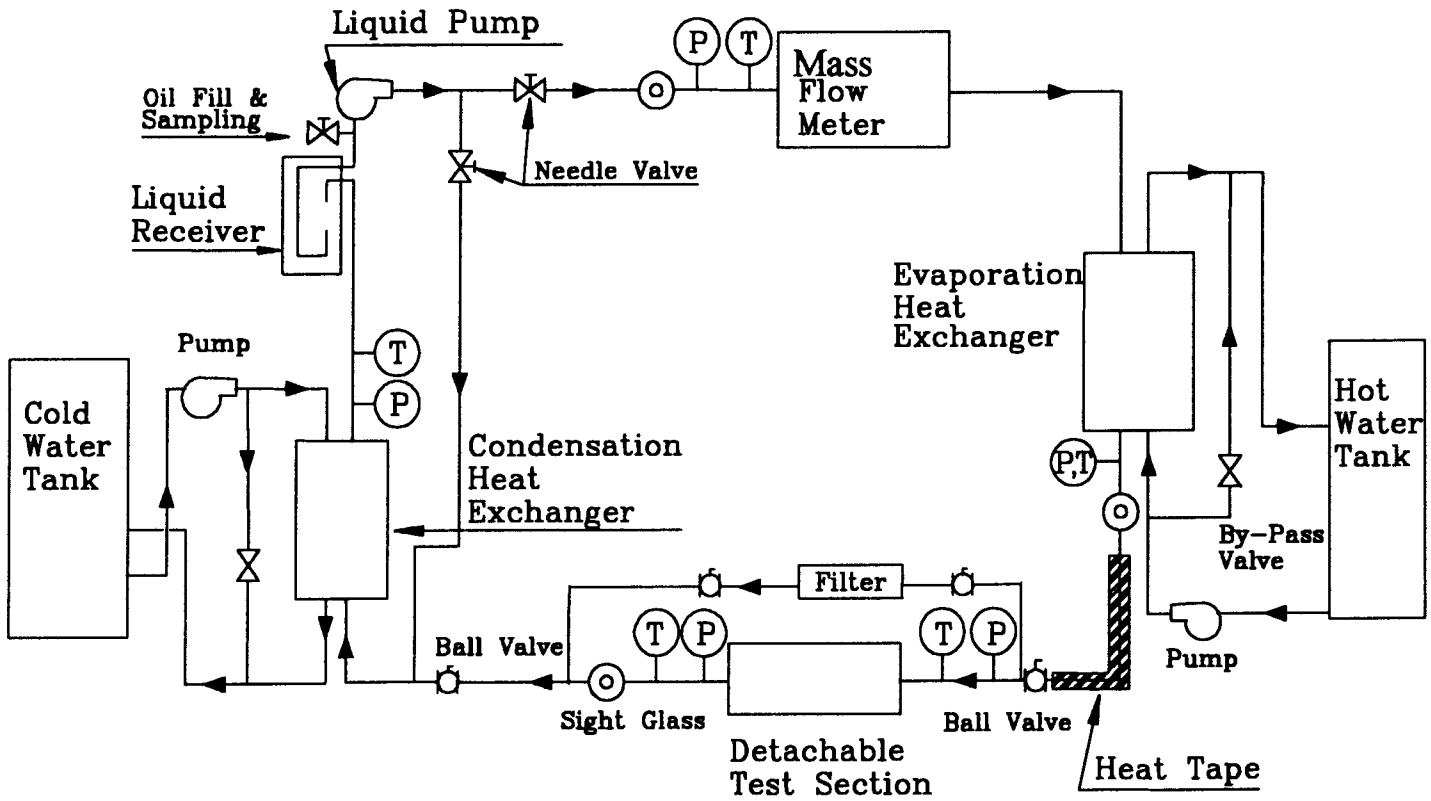

Figure 2.1: Schematic Diagram of the Short Tube Test Setup.

conditions at the inlet of the test section, most of the energy transfer to the refrigerant was supplied by the evaporation heat exchanger. A heat tape with adjustable output from 0 to 3071 Btu/h (0.9 kW) was utilized to provide precise control of upstream subcooling. For two-phase flow conditions at the inlet of the test section, the flow from the pump was heated by the evaporation heat exchanger to 2°F (1.1°C) of subcooling, and a heat tape was used to reheat the refrigerant to the desired inlet quality. A hot water loop supplying water to the evaporation heat exchanger consisted of a residential water heater and a centrifugal pump. Water flow rates were controlled by both a throttling valve and a by-pass valve. The temperature of the water entering the heat exchanger was monitored using a thermocouple and adjusted by a mechanical thermostat.

The heat tape was mounted along an eight foot (2.44 m) section of refrigerant tubing after the evaporation heat exchanger. To prevent heat loss to the ambient, the heat tape was insulated with 9 in. (22.9 cm) thick rubber insulation. Six thermocouples were placed inside and outside of the insulation to calculate the overall heat transfer coefficient for heat loss. For two-phase entering the test section, the power input into the heat tape was measured using a watt transducer. Liquid refrigerant temperature entering the heat tape section plus inside and outside insulation temperatures were also measured. The refrigerant enthalpy at the inlet of the test section was calculated by performing an energy balance of the power input into the heat tape, heat loss through the insulation, and enthalpy at the inlet of the heat tape. The enthalpy at the inlet of the heat tape, which was always subcooled, was determined from the measured temperature and pressure. The quality of the refrigerant flow entering the test section was calculated from the enthalpy and the measured pressure at the inlet of the test section.

After all upstream conditions were established, the flow entered the test section. The pressure and temperature were measured upstream and downstream of the short tube. Flow

conditions were also monitored using a sight glass at the exit of the short tube. A filter-dryer was mounted in the by-pass line of the test section and was used prior to collection of data.

Two-phase refrigerant exiting the test section was condensed and subcooled in the water/glycol cooled heat exchanger (condensation heat exchanger) so that the refrigerant pump had only liquid at its suction side. A liquid receiver was used before the refrigerant pump to ensure only liquid entered the pump. The pressure at the exit of the test section (downstream or evaporator pressure) was controlled by adjusting the temperature and flow rate of chilled water/glycol entering the heat exchanger. The water-glycol loop consisted of a 170 gal (644 L) insulated storage tank, 3 ton (10.6 kW) chiller unit, a centrifugal pump, and a by-pass line concentric tube heat exchanger. The concentration of glycol in the water was 50 %. The water/glycol mixture was cooled to 3°F (-16°C) by the chiller. The mass flow rate of the mixture was metered using a throttling valve and by-pass line. The temperature of the storage tank and the supplied mixture to the heat exchanger were monitored by a thermocouple.

Short Tube Description

The orifice test section located between the heat tape and condensation heat exchanger was designed to allow fast orifice replacement. The current testing utilized short tube orifices having a length of 0.5 in. (12.7 mm), 0.75 in (19.05 mm), and 1.0 in (25.4 mm) and no entrance chamfering. The orifice diameters were selected to correspond to commercially available short tubes in residential air conditioners or heat pumps.

Figure 2.2 shows the schematic of the orifice test section for routine performance tests. The short tube was made from brass which was bored and reamed to insure a smooth surface. The short tubes were fixed between two 0.375 in. ± 0.005 in.(9.53 mm ± 0.13 mm) O.D. × 8 in. ± 0.5 in. (20.32 cm ± 1.27 cm) long copper tubes using soft solder. The test

section was mounted into the test loop using Swagelok connections which provided ease of installation and replacement.

The short tubes used in this investigation are listed in Table 2.1. Short tube diameters were measured using a precise plug gauge set with 0.0005 in. (0.013 mm) increment of diameter. The precision error of the diameter measurement was estimated at ±0.0005 in. (0.013 mm). Short tube lengths were measured with a dial caliper which had a ±0.0005 in. (0.013 mm) accuracy.

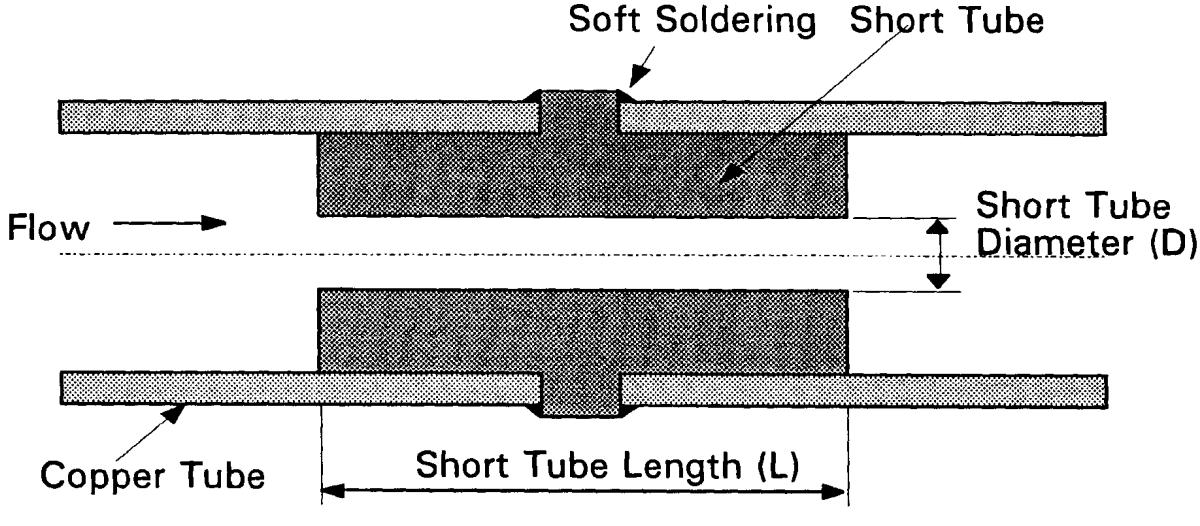

Figure 2.2: Schematic of a Short Tube Test Section for Routine Performance Tests.

Table 2.1: Dimensions of the Test Sections

Refrigerant	Diameter, in.(mm)
Ternary: R32/R125/R134a (23%/25%/52%)	① 0.0432 (1.09) ② 0.0528 (1.34) ③ 0.0676 (1.72) ④ 0.0763 (1.94)
Binary: R32/R125 (50%/50%)	① 0.0432 (1.09) ② 0.0528 (1.34) ③ 0.0676 (1.72) ④ 0.0763 (1.94)

Oil Injection and Sampling

The lubricant was injected into the suction side of the refrigerant pump using an air-cylinder in a batch process. The testing sequence proceeded from pure refrigerant to oil and refrigerant mixtures. The amount of the lubricant injected was calculated from the rod displacement and the diameter of the cylinder. The weight of the lubricant batch was also monitored to inject the required amount of oil using an electronic scale accurate to ±0.02 lb (10.0 g).

Oil concentration was determined by sampling. The schematic of the sampling vessel and filter assembly is shown in Figure 2.3. The sampling vessel was cylindrical and had an inside diameter of 5 in. (12.7 cm) and a length of 12 in. (30.5 cm). The volume of sampling vessel was large compared to the volume of the sample to ensure low vapor velocity during the distilling procedure so that no oil particles could leave with the vapor. The amount of refrigerant-lubricant mixture sampled from the suction side of the pump was approximately one pound (0.454 kg). During the sampling process, the sample weight entering the vessel was monitored using a scale accurate to ± 0.002 lb (± 1.0 g). After sampling, the refrigerant

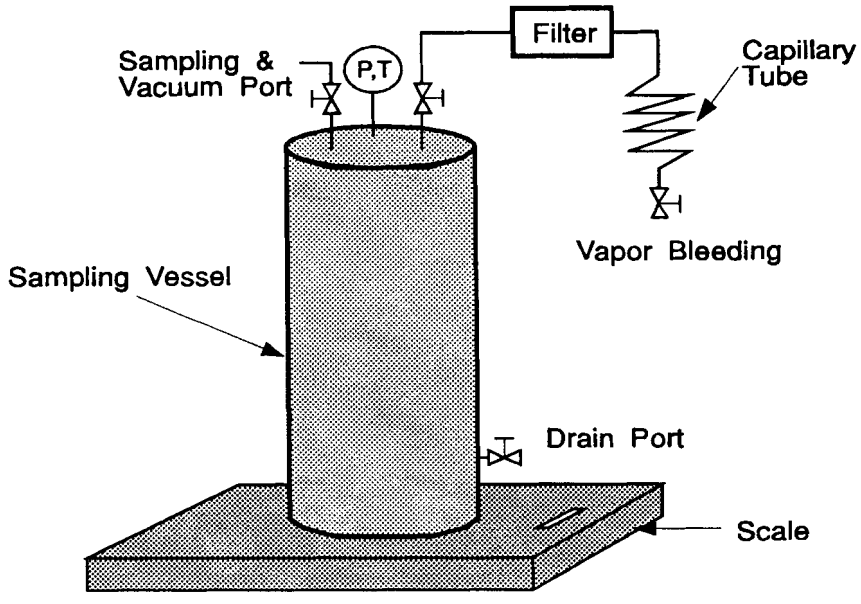

Figure 2.3: Schematic of the Sampling Vessel and Filter Assembly.

was removed from the sampling vessel by slowly bleeding the refrigerant vapor through a bleeder assembly which included a filter and a capillary tube 10 ft (3.05 m) long × 0.025 in. (0.64 mm) bore to catch any entrained oil in the exiting refrigerant. After bleeding, the cylinder was evacuated to remove any dissolved refrigerant in the lubricant. Based on the measurement of the empty weight of the cylinder and filter assembly, the weight immediately after sampling, and the weight after bleeding off the refrigerant, the oil concentration in the refrigerant was calculated. The procedure for calculating the oil concentration was based on ASHRAE Standard 41-4-1984 (ASHRAE 1984). According to this method, oil concentration could be calculated by one of two methods. The first method, known as the sample basis calculation, determined oil concentration based upon the mass of the oil and refrigerant. The second method determined oil concentration based upon the pure refrigerant basis. Both methods are described by the following equations:

Method 1 : $$C_s = \frac{m_f - m_i}{m_t - m_i} \quad (2.1)$$

Method 2 : $$C_r = \frac{m_f - m_i}{m_t - m_f} \quad (2.2)$$

where: m_i = initial vessel weight
m_o = weight of the oil
m_t = total weight of vessel, refrigerant and oil
m_f = total weight of vessel and oil

All quantities reported in this report are based upon Method 2.

Instrumentation

Temperatures, pressures, flow rate, and power input were monitored in the test loop using a computer and data acquisition system. Each sensor was calibrated before being connected to the data logger to reduce experimental uncertainties.

All temperature measurements were made using copper constantan thermocouples. The total error of the temperature measurement was estimated at ±0.72°F (0.4°C). Calibration of a thermocouple was performed by adjusting a potentiometer located on each isothermal block of the input card (the zero point was set using the ice bath). After making a thermocouple junction, the thermocouple was calibrated in a constant temperature bath. Six thermocouple probes were mounted in the refrigerant line to measure accurately the refrigerant temperature. The probes with 1/16 in. (1.59 mm) O.D. were inserted far enough into the flow of the refrigerant to minimize the conduction effects of the copper tube (Figure 2.4).

Six pressure transducers were used in measuring the refrigerant pressures. Each pressure transducer was calibrated with a standard dead weight tester . The pressure

transducers in the refrigerant line were installed with ball valves to allow easy disassembly without any loss of the refrigerant in the system.

The refrigerant mass flow rate was measured with a Coriolis effect mass flow meter. The precision of the flow meter was ±0.4% of full scale [26 lb/min (11.8 kg/min)]. Hot water was used as a calibration liquid because hot water has approximately the same kinetic viscosity as the refrigerants. Therefore, the error in the measurement of the mass flow rate caused from the viscosity difference between refrigerants and a calibration liquid can be assumed negligible (Tree 1970). Calibration was performed by measuring the weight of water flowing into a measuring tank per unit time.

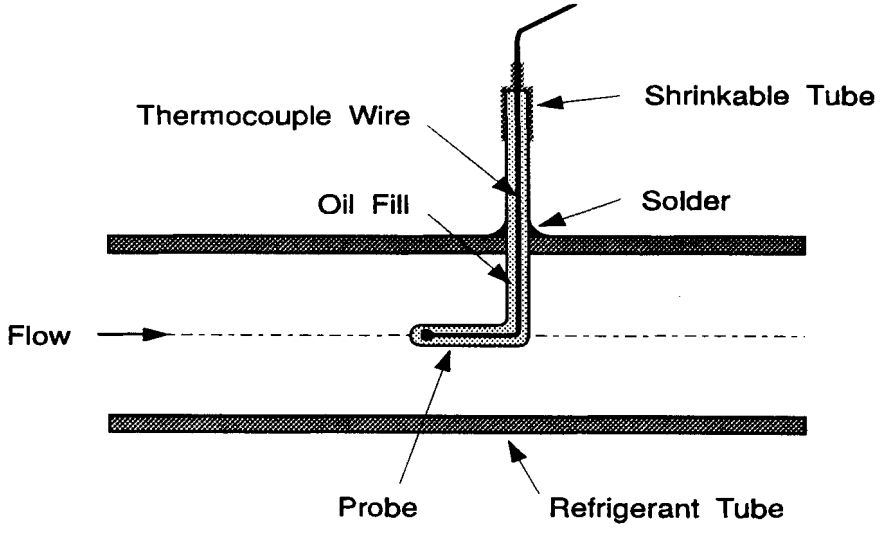

Figure 2.4: A Typical Refrigerant Line Temperature Probe.

A voltage transformer and a watt transducer were utilized to measure the power input into the heat tape. A watt transducer was calibrated using a standard voltmeter and ampere meter. Estimated experimental uncertainty was ±0.5% full scale (5118 Btu/h (1.5 kW)) accuracy.

The two-phase quality at the inlet of the short tube was determined by applying an energy balance to the heat tape at the entrance of the short tube. The uncertainty of the quality was estimated using the Kline and McClintock (1953) error method. Based on sample calculations, the uncertainties of the qualities were less than 4% of calculated qualities.

Data Acquisition

The data acquisition was done with a personal computer and an Acurex (Model Autocalc) data logger. Sensor signals from the test points listed in Table 2.2 were collected and converted to engineering units by a data logger which handled millivolt and milliamp signals as well as voltages and frequency signals. During the test, the data processed by the data logger were transferred to a personal computer where they were displayed continuously on the screen and stored on a hard disk. The scan rate was adjustable, so the data were collected every six seconds. Before the final data were collected, all operating parameters were monitored on the screen to check establishment of the required conditions.

After completion of the test for each short tube, the data reduction program, which was written in QuickBASIC, was used to calculate properties for analysis. Thermodynamic properties for the ternary zeotrope and binary near-azeotrope were calculated based upon thermodynamic property data supplied by the refrigerant manufacturers.

Table 2.2: Description of the Data Acquisition Sensor Channels.

Channel	Sensor Type	Location
00	Pressure Transducer	Short Tube Inlet
01	Pressure Transducer	Short Tube Exit
04	Pressure Transducer	Liquid Receiver Inlet
05	Pressure Transducer	Flow Meter Inlet
06	Pressure Transducer	Flow Meter Exit
07	Pressure Transducer	Upstream of Heat Tape
08	Flow Meter	Liquid Pump Exit
09	Watt Transducer	Heat Tape
10	Thermocouple-Probe	Short Tube Inlet
11	Thermocouple-Probe	Short Tube Exit
14	Thermocouple-Probe	Liquid Receiver Inlet
15	Thermocouple-Probe	Flow Meter Inlet
16	Thermocouple-Probe	Flow Meter Exit
17	Thermocouple-Probe	Upstream of Heat Tape
18-23	Thermocouple	Heat Tape Insulation
44	Mass Flow Meter	Liquid Pump Exit

CHAPTER III

EXPERIMENTAL PROCEDURE

A series of experiments for each refrigerant was run to investigate the influence of the operating parameters on the mass flow rate though the short tubes. Two types of experiments were performed: (1) measurement of the mass flow for the pure refrigerants and (2) measurements of the effects of oil concentration on performance. Conditions were chosen to cover a wide range of operating conditions for a short tube expansion device found in a typical residential heat pump or air-conditioner.

The experimental variables controlled included: (1) upstream subcooling or quality, (2) upstream pressure, (3) downstream pressure, and (4) orifice geometry. Operating pressures for the short tubes tested were selected based upon several condensing temperatures. Nominal condensing temperatures 95°F (35.0°C), 110°F (43.3°C), and 125°F (51.7°C) were selected for both the ternary and binary refrigerants. The corresponding upstream saturation pressures for the ternary mixture were 221 psia (1524.kPa), 271 psia (1870 kPa), and 329 psia (2271 kPa). The binary mixture had corresponding upstream saturation pressures of 310 psia (2136kPa), 380 psia (2618 kPa), and 461 psia (3176 kPa). Downstream pressures were selected based upon evaporating temperatures of 30°F (-1.1°C), 40°F (4.4°C), and 50°F (10.0°C) for both the ternary and binary refrigerants.

Upstream conditions were varied by altering the degree of subcooling of the refrigerant for single phase tests and altering the quality for two-phase tests. Oil tests for the binary and ternary mixtures were performed with oil concentrations on a mass basis ranging from 0% to 2.15%. The lubricant was Mobil RL32S (32 centistokes) polyol ester. Conditions for each test were a combination of operating variables listed in Table 3.1.

Approximately 32 tests were completed for the pure refrigerants for each short tube diameter. The downstream pressure for the oil tests were set at the median pressure used to test the pure refrigerants. Oil tests were conducted for each orifice at all subcooling levels and upstream pressures, but only the median downstream pressure was tested.

The data developed from the measurements included refrigerant flow rate, pressure drop across the short tube, and upstream subcooling/quality. Data were taken at steady state. Several criteria had to be met for the data to be accepted. The controlling parameters had to be within the following limits: upstream pressure, ±1.0 psia (7 kPa); downstream pressure, ±2.0 psia (14 kPa); upstream temperature ±0.72°F (0.4°C); and quality, ±0.3%. When the flow rate was insensitive to downstream pressure, the downstream pressure limit was set to ±5.0 psia (34 kPa) to allow faster stabilization of the flow conditions.

The setup was allowed to reach steady state while satisfying required operating conditions before the final data acquisition was started. The establishment of steady state was checked by monitoring the operating conditions and mass flow rates. When the system came to steady-state, data were collected every six seconds for a period of four minutes. The data for each channel were then averaged over four minute intervals.

Table 3.1: Test Conditions

Refrigerant	Upstream Pressure, psia (MPa)	Downstream Pressure, psia (MPa)	Subcooling or Quality	Oil Mass Percent
Ternary: R32/R125/R134a (23%/25%/52%)	221 (1.53)	78 (0.54)	20°F (11.1°C)	0%
	271 (1.87)	94 (0.65)	10°F (5.6°C)	1.0%
	329 (2.27)	111 (0.76)	5°F (2.8°C)	
			0°F (0°C)	
			5.0 %	
Binary: R32/R125 (50%/50%)	310 (2.14)	114 (0.78)	20°F (11.1°C)	0%
	380 (2.62)	135 (0.93)	10°F (5.6°C)	2.15%
	461 (3.18)	160 (1.10)	5°F (2.8°C)	
			0°F (0°C)	
			5.0 %	

After finishing a series of the tests for a short tube, the test section was replaced with a new test section. The replacement of the test section was conducted by closing the ball valves before and after the existing test section to shut off the refrigerant flow and opening the bypass around the test section. After changing the test section, the space between the ball valves was evacuated. Flow through the test section was re-established by opening the ball valves and closing the bypass ball valves. The bypass line made it possible to re-route refrigerant flow without shutting the system down, thus saving time in reaching steady state with the new test section.

The composition of the ternary and binary refrigerant mixtures was checked by performing a gas chromatograph (GC) analysis on small samples from the system taken during testing. Samples were taken from the high pressure liquid side of the system. A summary of the GC results is presented in Table 3.2. The zeotropic ternary mixture showed some variation in composition between the liquid and vapor phases. Further sampling for the ternary mixture confirmed the variation in composition seen in the summary data presented in Table 3.2. The azeotropic binary mixture consistently yielded compositions as shown in the table below.

Table 3.2: Summary of Gas Chromatograph Tests*

Refrigerant	Mass Percentages	Sample Source
R32/125/134a	(25.1 / 25.7 / 49.2)	Cylinder
	(24.3 / 27.7 / 48.1)	System
R32/125	(51.4 / 48.6)	Cylinder
	(53.1 / 46.9)	System

* Refrigerant composition tolerances were set at ±4% for all tests.

On completion of the tests with a refrigerant, the system was discharged and then evacuated. The system was flushed with R-134a and then evacuated again for several hours. This flush/evacuate procedure was repeated for a total of two cycles. The system was then charged with the required amount of the replacement refrigerant, which was around 15 lb (7 kg). After a series of test runs were made with the first short tube to verify charge levels, the system was ready for further testing.

Oil was injected into the suction side of the pump (the detailed procedure was described in the section "Oil Injection and Sampling"). Before sampling of the refrigerant-lubricant mixture, the system was operated for three hours to allow the refrigerant and lubricant to fully mix. The sampling and calculation procedure for oil concentration was based on ASHRAE Standard 41-4-1984 (ASHRAE 1984).

For two-phase flow conditions at the inlet of the test section, the quality was determined from the energy balance on the heat tape. The overall heat transfer coefficient, *UA*, for the insulation section was determined from measured data for single-phase flow conditions and an energy balance on the test section.

$$UA = (Q_H - Q_r)/(T_{o,m} - T_{i,m}) \tag{3.1}$$

$$Q_r = \dot{m}_r (h_{o,r} - h_{i,r}) \tag{3.2}$$

$$Q_L = Q_H - Q_r \tag{3.3}$$

Where Q_H is power input to the heat tape, Q_r is the rate that heat energy is transferred to the refrigerant, Q_L is the rate that heat energy is lost through the insulation, and $T_{i,m}$ and $T_{o,m}$ are the mean temperatures at the inside and outside of the insulation, respectively. Based on the overall heat transfer coefficient and measured data for two-phase conditions, the enthalpy at the exit of the heat tape was determined by:

$$Q_L = UA(T_{o,m} - T_{i,m}) \tag{3.4}$$

$$h_{o,r} = \frac{Q_H - Q_L}{\dot{m}_r} + h_{i,r} \tag{3.5}$$

Finally, the quality was evaluated from the enthalpy calculated using Equation (3.5) and the pressure at the inlet of the test section. The overall heat transfer coefficients were checked by comparing the results of Equation (3.1) with the curve fitted results as a function of power input and mean operating temperature of the insulation. The maximum difference between these two methods was within ±2.0%.

CHAPTER IV

EXPERIMENTAL RESULTS FOR R32/125/134a (23%/25%/52%)

The ternary refrigerant mixture of R32/125/134a (23%/25%/52%) (Tradename AC9000) was tested in the apparatus as described in chapter two. Test conditions for all tests were a combination of condensing temperatures ranging from 95°F (35.0°C) to 125°F (51.7° C) and evaporating temperatures ranging from 30°F (-1.1°C) to 50°F (10°C). Short tube orifices of length 0.5 in (12.70 mm), 0.75 in (19.05 mm), and 1 in (25.4 mm) with diameters ranging from 0.0432 in (1.09 mm) to 0.0763 in (1.94 mm) were tested at all condensing and evaporating conditions. The following describes the results for the ternary refrigerant mixture (AC9000) for the stated flow conditions and oil contamination mass percentages.

PURE R32/125/134a (23%/25%/52%)

The following section discusses the effects of downstream pressure, upstream subcooling/quality, upstream pressure, diameter, and length on the mass flowrate of refrigerant through a given orifice geometry. Appropriate figures are also introduced to represent the effects of varying the above parameters on the mass flowrate through the short tube.

Effects of Downstream Pressure on Mass Flowrate

When the upstream pressure was less than the saturation pressure corresponding to the given upstream temperature, the mass flowrate of refrigerant was generally insensitive to a change in downstream pressure (Figure 4.1). Mass flowrate varied by less than 2% from its value at the highest downstream pressure tested. For upstream pressures below the saturation

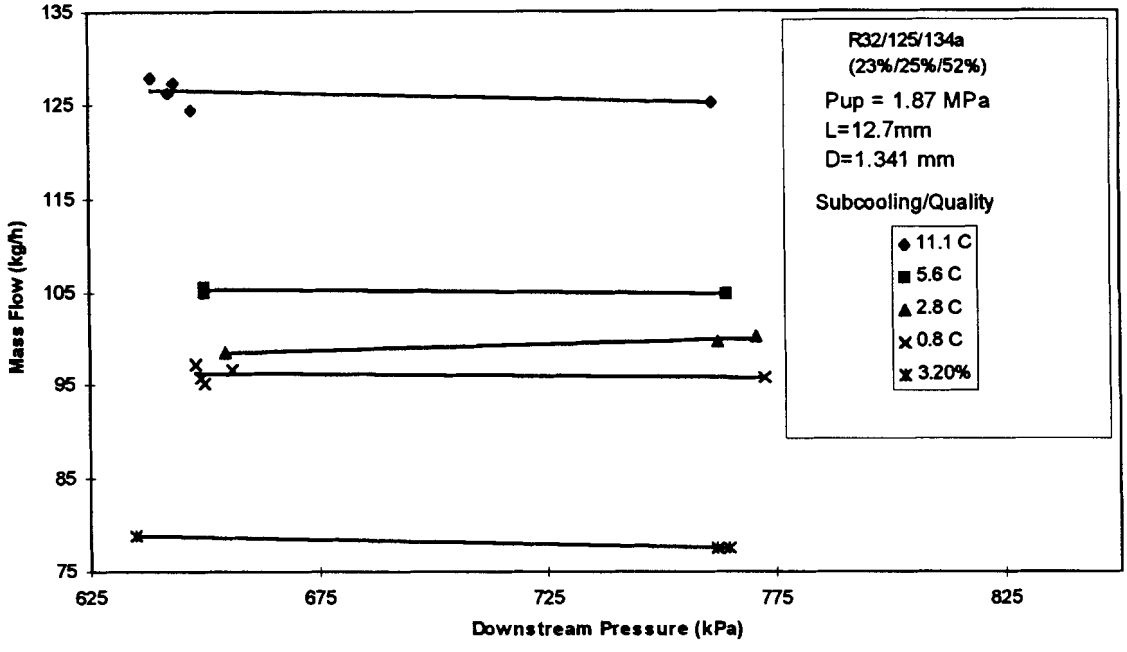

Figure 4.1: Flow dependency on downstream pressure for a short tube with length 0.5 in and diameter of 0.0528 in.

pressure, approximate choking flow conditions were typically established in the short tube orifices. All downstream pressures were below the saturation pressure corresponding to the upstream temperature.

Because heat pumps and air conditioners operate at evaporating pressures lower than the saturation pressure, approximately choked flow would be the main operating condition for all upstream temperatures. Figure 4.1 was typical of the behavior of the other orifices tested at different downstream pressures. For all subcooling levels and two-phase qualities tested in the present study, the mass flowrate was almost constant as the downstream pressure was decreased below the saturation pressure corresponding to the upstream temperature. For a short tube with a length of 0.5 in (12.7 mm) and diameter of 0.0528 in (1.34 mm), mass flowrate varied by less than 2% for all subcooling levels and qualities. These trends were observed in the previous research (Kim, 1993; Aaron and Domanski, 1990).

Effects of Upstream Subcooling/Quality

Figure 4.2 shows the mass flowrate as a function of subcooling/quality for three upstream pressures and all downstream pressures. The general trend seen in this figure was consistent with the previous results obtained for R22 and R134a (Kim and O'Neal, 1993a, 1993b). The refrigerant flowrate increased as the upstream subcooling increased, and decreased as the inlet quality increased. It should be noted that in Figure 4.2, there is a scale change due to the representation of percent quality as negative numbers.

Abrupt drops in flowrate were seen as inlet conditions progressed from saturated liquid (zero percent quality) into the saturation region. For an upstream pressure of 221 psia (1524 kPa), flowrate decreased 21% from 205 lb/h (93.2 kg/h) to 162 lb/h (73.4 kg/h) as the quality increased from 0% to 1.7%. For an upstream pressure of 271 psia (1870 kPa), flowrate decreased 18.5% from 210 lb/h (95.3 kg/h) to 171 lb/h (77.6 kg/h) as quality increased from 0% to 3.2%. These trends are consistent with the previous work performed by Kim and O'Neal (1993a, 1993b).

The variation of mass flowrate with subcooling/quality for several different diameters can be seen in Figure 4.3. As the diameter increased, the slope of the subcooling line increased. For two phase entering the short tube, the slope appeared to decrease slightly as the diameter was increased. In the subcooling region, the mass flowrate increased an average of 32.5% as subcooling varied from 0°F (0°C) to 20°F (11.1°C). In the two phase region, mass flowrate decreased an average of 18% as quality was increased from 0% to 2%.

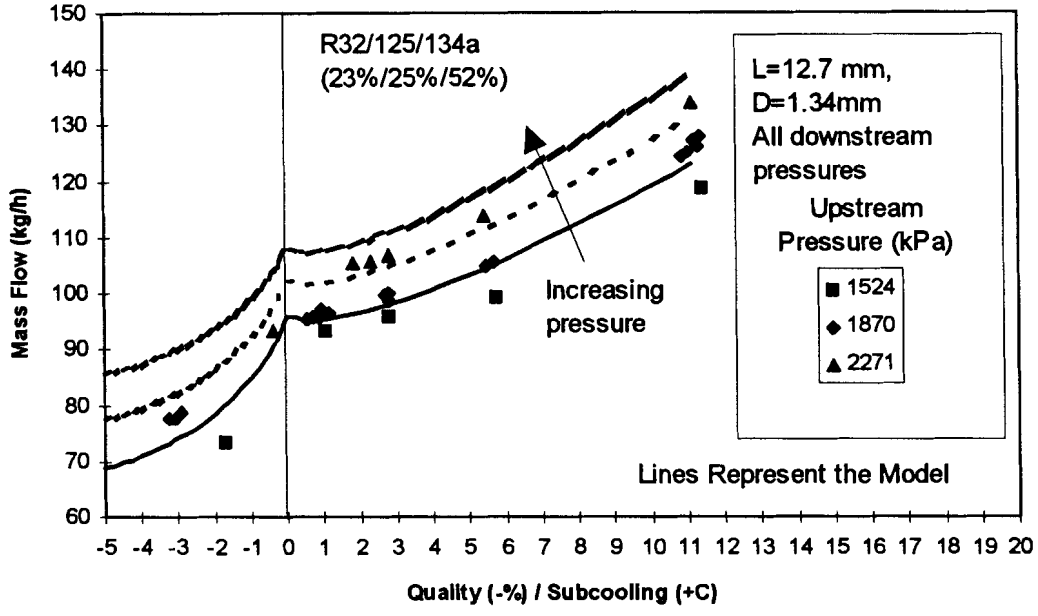

Figure 4.2: Flow dependency on subcooling/quality for three upstream pressures for a short tube with length 0.5 in (12.7 mm) and diameter of 0.0528 in (1.34 mm).

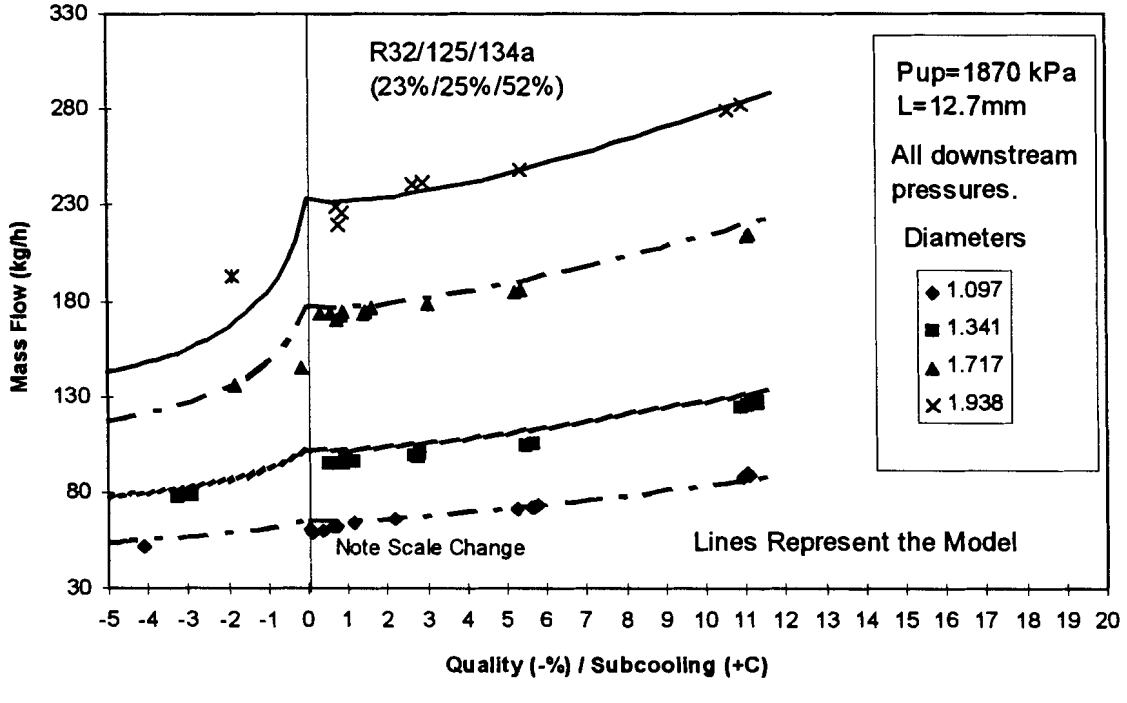

Figure 4.3: Flow dependency on subcooling/quality for three diameters and upstream pressure of 271 psia (1870 kPa) at all downstream pressures.

Effects of Upstream Pressure

Figure 4.4 shows the variation in mass flowrate with upstream pressure at different levels of subcooling/quality. As the upstream pressure was increased, the mass flowrate increased in a linear fashion. This trend was maintained even though the upstream pressure was as high as 329 psia (2271 kPa) corresponding to an evaporating temperature of 125°F (51.7°C). The slope of each line was approximately linear and increased with an increase in subcooling. This increase in slope appeared to decrease with an increase in diameter. For two phase at the inlet of the short tube, Figure 4.4 showed that mass flowrate averaged 18% lower than the mass flowrate at saturated conditions over the range of upstream pressures. (Please note that these figures include all downstream pressures.)

Effects of Short Tube Diameter

The variation in mass flowrate with short tube diameter is shown in Figure 4.5. The effects of the short tube diameter on flowrate was consistent with the results of R22 and R134a (Kim and O'Neal, 1993a, 1993b). For high subcooling the mass flowrate was proportional to the diameter squared. As the diameter increased, mass flow increased with slope increasing slightly with upstream pressure. This figure shows that the diameter strongly affected mass flowrate; therefore, it is necessary to accurately measure diameter in order to predict flowrate.

As upstream subcooling decreased (Figure 4.6), the effects of the short tube diameter on flowrate decreased. The data near the saturation temperature (near zero subcooling) tended to vary directly with the diameter. For two-phase flow entering the short tube, flowrate was almost linearly proportional to the short tube diameter. This suggested that any model of this behavior would need to correct for this variation in behavior near saturation and at various qualities.

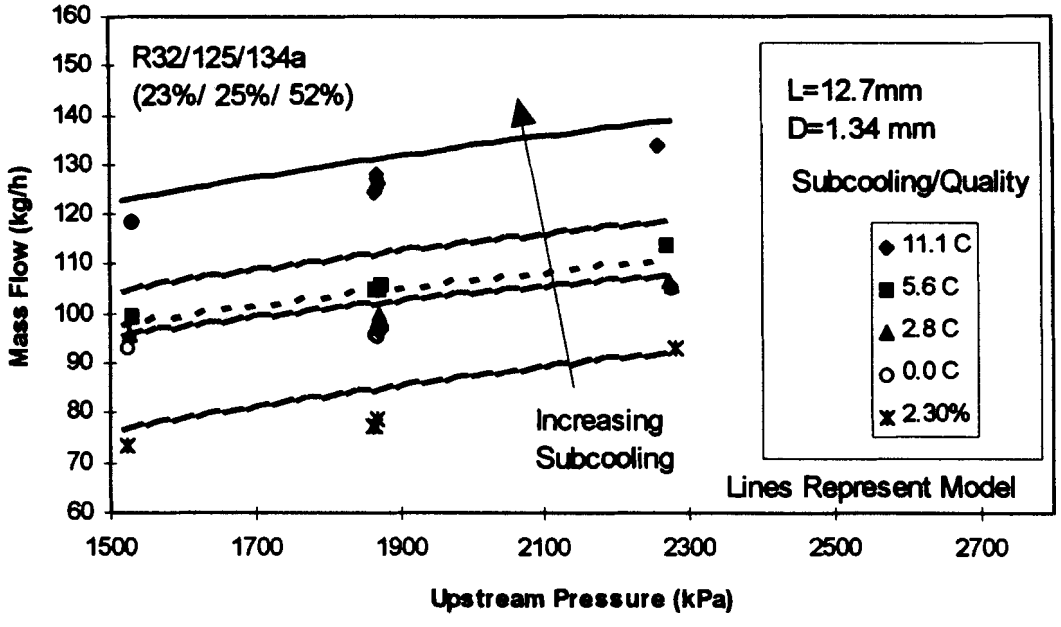

Figure 4.4: Flow dependency on upstream pressure as a function of upstream subcooling/quality for a short tube with length 0.5 in (12.7 mm) and diameter of 0.0528 in (1.341 mm).

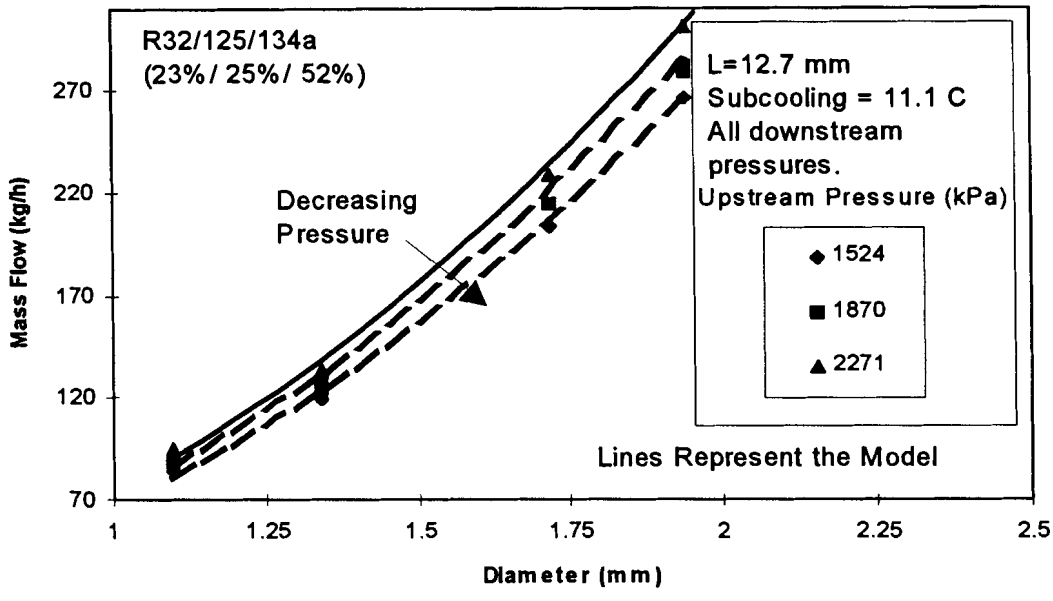

Figure 4.5: Flow dependency on short tube diameter for several upstream pressures and subcooling of 20°F (11.1 °C).

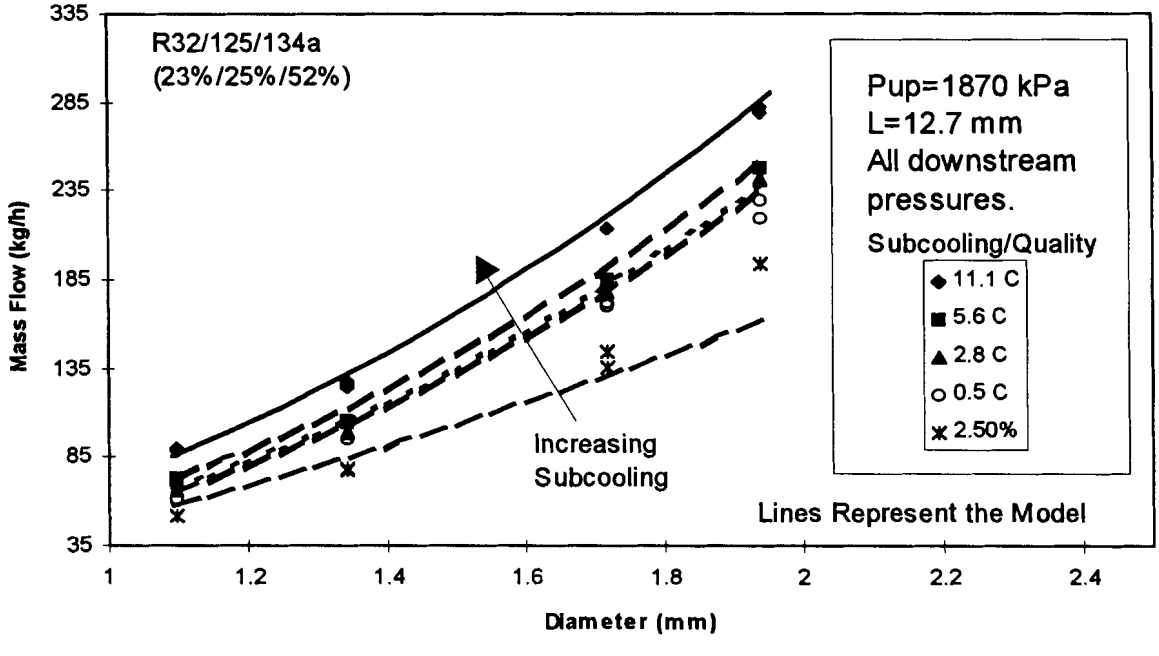

Figure 4.6: Mass flow as a function of diameter for upstream pressure of 271 psia (1870 kPa), length of 0.5 in (12.7 mm), and various levels of subcooling/quality.

Effects of Short Tube Length

Figure 4.7 shows the effects of increased short tube length on mass flowrate. As short tube length was increased from 0.5 in (12.7 mm) to 1.0 in (25.4 mm) mass flow decreased by an average of 9.5% from its value at the 0.5 in (12.7 mm) length. This decrease in mass flow with increasing length was more exaggerated at the lower subcoolings. For the orifice given in Figure 4.7, mass flow decreased from the value at 0.5 in (12.7 mm) by 3.3%, 8.4%, and 16.7% for subcoolings of 20°F (11.1°C), 10°F (5.6°C), and 2°F (1.8°C), respectively. The basic trends seen within this figure were consistent for all orifices tested.

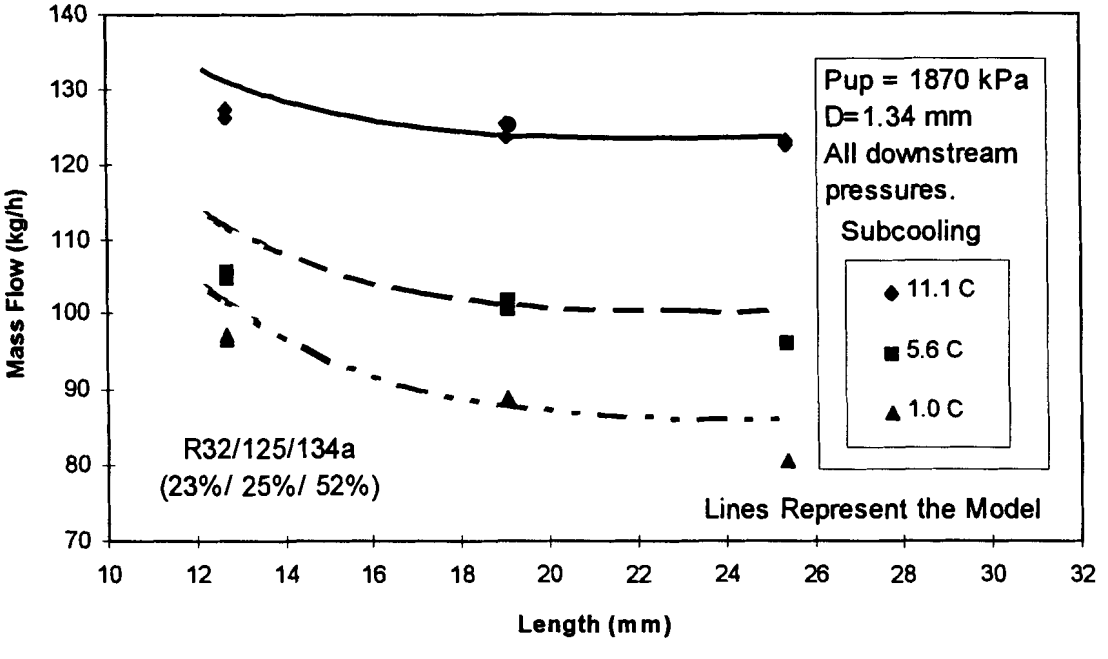

Figure 4.7: Effects of length on mass flow for upstream pressure of 271 psia (1.9 MPa) and diameter of 0.0528 in (1.341 mm).

MIXTURES OF OIL AND R32/125/134a (23%/25%/52%)

This section presents the experimental results obtained during examination of the flow characteristics of the ternary refrigerant mixture and oil through the various short tube orifices. Discussion with the advisory committee directed testing toward oil concentrations of 1% to 3%. It was agreed that oil concentrations of 1% to 3% were normally seen circulating in a heat pump or air-conditioning system. The mass percentage of oil was set at 1.0% for testing of all the short tube diameters at all upstream pressures and the median downstream pressure which corresponded to evaporating conditions of 40°F (4.4°C). The mass flowrate ratio, m_R ,was calculated to compare the mass flowrate of pure refrigerant and oil/refrigerant mixtures. The mass flow ratio, m_R , was defined as:

$$m_R = \frac{\text{mass flowrate of oil and refrigerant mixture}}{\text{mass flowrate of pure refrigerant}} \tag{4.1}$$

General Trends

Figures 4.8 and 4.9 show the effects of oil concentration on mass flowrate for a given geometry with a range of subcoolings/qualities and upstream pressures. These figures revealed that the mass flowrate remained within 5% of the pure value at all upstream pressures and subcoolings. For twophase flow at the entrance of the short tube, the addition of oil to the refrigerant mixture increased mass flow by more than 12%. Previous research showed that increasing the oil concentration beyond a certain percentage would cause mass flow to drop sharply. Generally, mass flow would drop sharply for oil concentrations greater than 2% to 2.5% in keeping with trends observed for R134a.

Figure 4.9 showed the effects of upstream pressure and oil concentration on the mass flow ratio for a fixed upstream subcooling of 10 °F (5.6 °C). The trends plotted show that the

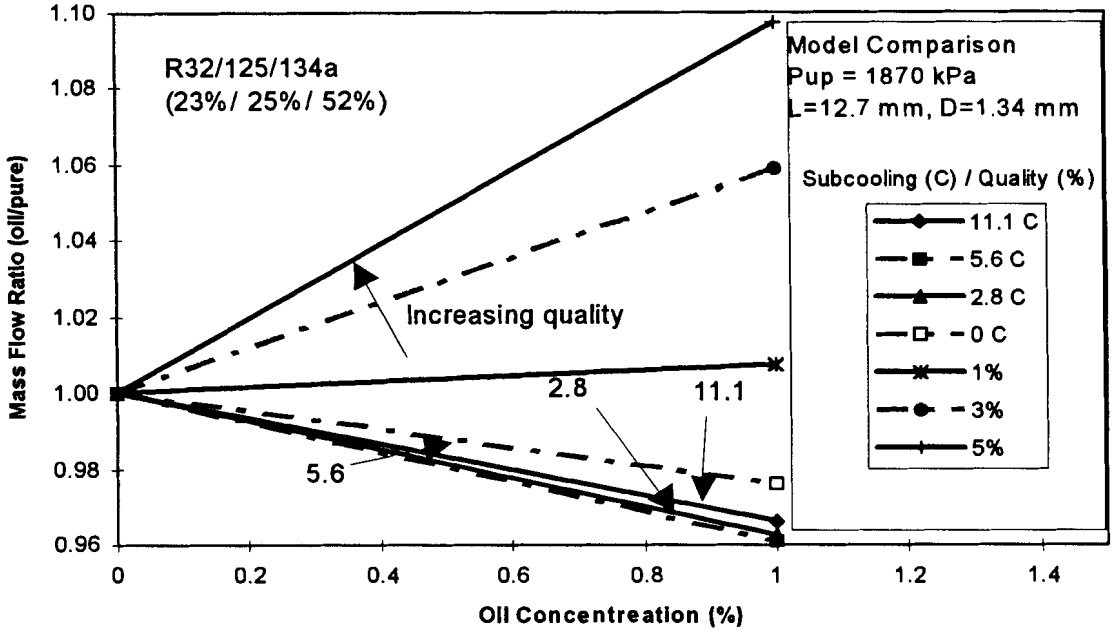

Figure 4.8: Mass flow ratio as a function of oil concentration for upstream pressure of 271 psia (1870 kPa), length of 0.5 in (12.7 mm), diameter of 0.0528 in (1.34 mm), and several subcoolings/qualities.

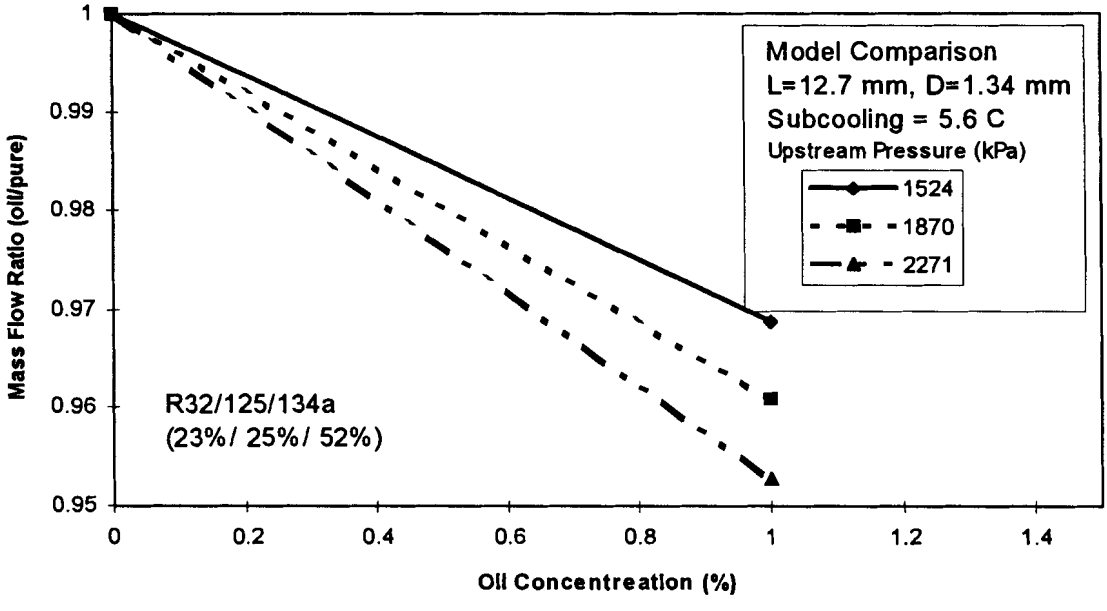

Figure 4.9: Mass flow ratio as a function of oil concentration for all upstream pressures with length of 0.5 in (12.7 mm), diameter of 0.0528 in (1.34 mm), and subcooling of 10 °F (5.6 °C)

mass flow ratio is lower for the higher upstream pressures. For the upstream pressure of 221 psia (1524 kPa), the mass flowrate was reduced by 3.1% compared to a reduction of less than 4.7% for an upstream pressure of 329 psia (2271 kPa).

Effects of Upstream Subcooling/Quality

Figure 4.10 shows the variation in mass flowrate as a function of upstream subcooling for a fixed geometry and a range of upstream pressures. At high levels of subcooling, the addition of oil decreased flowrate from the pure case by approximately 3%. For the given oil concentration, a decrease in upstream subcooling caused a decrease in mass flow. The mass flow ratio at an upstream pressure of 221 psia (1524 kPa) decreased by approximately 2% as upstream subcooling dropped from 20°F (11.1°C) to saturated conditions.

Effects of Upstream Pressure

The flow dependency of the oil/refrigerant mixture upon upstream pressure can be seen in Figure 4.11. The mass flowrate increased with increasing upstream pressure even for the oil contaminated refrigerant. One possible explanation for the lower mass flow ratio at the higher upstream pressures could be the missibility of the oil in the refrigerant at the higher temperatures. Even though subcooling was constant for a given line in Figure 4.11, higher upstream pressures meant higher upstream temperatures. Mass flowrates for the 20°F (11.1°C) subcooling level were generally within ±3% of pure refrigerant flowrates. For subcooling levels below 10°F (5.6°C), the addition of oil tended to decrease the mass flowrate more rapidly than at higher subcooling levels (Figure 4.11). On average flowrates decreased by 3.5% for subcoolings below 10°F (5.6°C). Similar trends were observed in the previous work on R-134a (Kim, 1993). Twophase conditions at the short tube entrance showed that the addition of oil caused flowrate to decrease by a maximum of 9% with the average reduction being 6%.

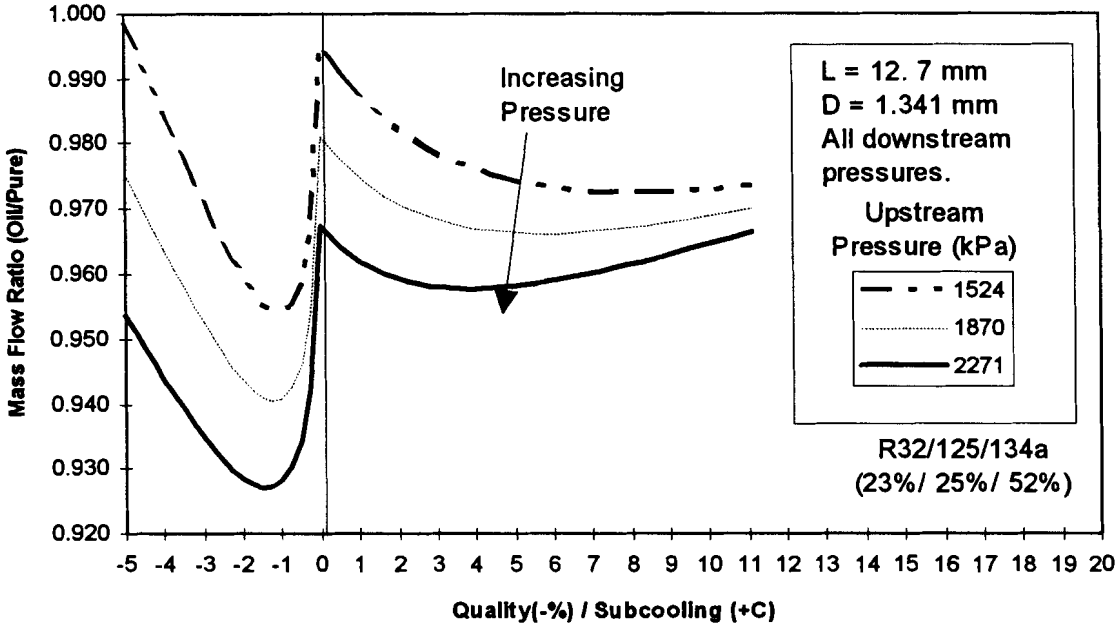

Figure 4.10: Mass flow ratio as a function of upstream subcooling for several upstream pressures.

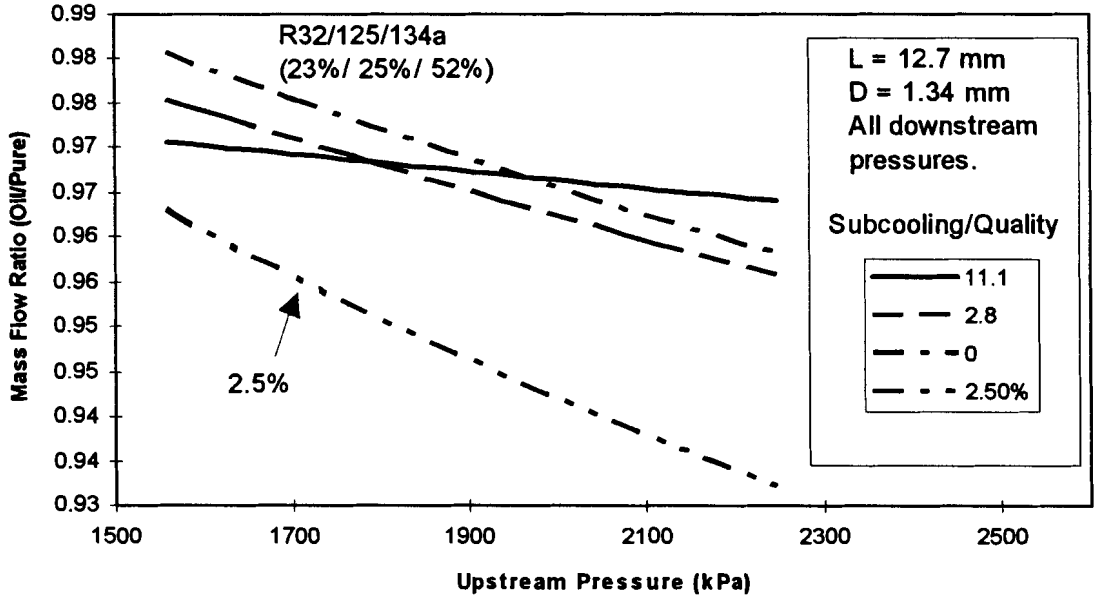

Figure 4.11: Mass flow ratio as a function of upstream pressure for all upstream subcoolings and 1% oil.

SUMMARY OF RESULTS FOR R32/125/134a (23%/25%/52%)

For the conditions of the present study, the existence of choked flow conditions was verified from plots of the mass flowrate of refrigerant as a function of downstream pressure. It was noted that weak establishment of choked flow may not promote system reliability and constant control.

Upstream pressure was also examined as a dominant parameter affecting the mass flowrate of refrigerant through the short tube orifice. As upstream pressure was increased, mass flow increased in a linear fashion. The increase in the slope of the mass flow/upstream subcooling line tended to decrease slightly with increases in short tube diameter. Increases in upstream subcooling also tended to cause increases in mass flowrate for a given upstream pressure.

The variation in refrigerant mass flowrate with short tube diameter for the ternary refrigerant mixture followed the same trends seen for the flow of R-22 and R-134a. For high subcooling, the mass flowrate varied with approximately the square of the orifice diameter. At subcooling levels near zero, the changes in flowrate with diameter were less pronounced. For two-phase conditions at the short tube entrance, the flowrate was almost linearly proportional to diameter.

The addition of oil to the ternary refrigerant had little effect on mass flowrate at higher subcooling levels. The flowrate generally remained within 5% of the pure case at subcooling levels of 20°F (11.1°C). If oil concentrations were increased further, the rapid drop in mass flow seen in past tests with R22 and R134a may have been more evident. The variations in flowrate with upstream pressure followed the same trends seen in the pure case. Increases in upstream pressure caused a linear increase in the mass flowrate. However, the rate of increase was lower for the oil/refrigerant mixture.

CHAPTER V

EXPERIMENTAL RESULTS FOR R32/125 (50%/50%)

The (near) azeotropic refrigerant R32/125 (50%/50% on a mass percentage) was tested in critical flow through short tube orifices of length 0.5 in (12.7 mm), 0.75 in (19.05 mm), and 1.0 in (25.4 mm) with diameters ranging from 0.0432 in. (1.09 mm) to 0.0763 in. (1.94 mm). Simulated condensing temperatures ranged from 80°F (26.7°C) to 125°F (51.7° C) with evaporating conditions of 30°F (-1.11°C) to 50°F (10.0°C). Upstream pressure corresponding to the various condensing temperatures ranged from a peak value of 461 psia (3176 kPa) to 310 psia (2136 kPa). Downstream pressure, upstream pressure, upstream subcooling/quality, short tube diameter, and short tube length were studied to determine their effects on refrigerant mass flowrate.

PURE R32/125 (50%/50%)

The following sections describe the effects of the above parameters on refrigerant mass flowrate through the short tube orifice. The figures introduced below represent the general trends in mass flow for the conditions under consideration.

Effects of Downstream Pressure on Mass Flowrate

For the case of the binary refrigerant, upstream pressures averaged much higher than the saturation pressure corresponding to the given upstream temperature. This meant that approximately choked flow conditions existed for all tests. Figure 5.1 shows the variation in mass flowrate with downstream pressure for all subcooling/qualities. At subcooling levels of 20°F (11.1°C), mass flowrate varied by less than 0.25% over the range of downstream pressures. These figures showed that for the high operating pressures of the binary

refrigerant, approximately choked conditions were well established at all downstream pressures visited in the normal operating ranges of heat pumps and air-conditioners.

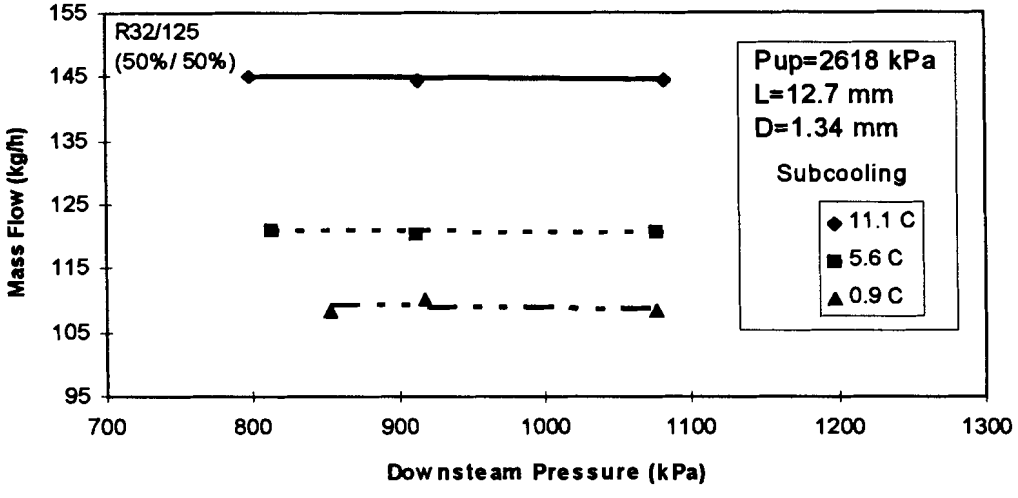

Figure 5.1: Flow dependency on downstream pressure for a short tube of length 0.5 in (12.7 mm) and diameter of 0.0528 in (1.341 mm) with upstream pressure of 380 psia (2618 kPa).

Effects of Upstream Subcooling/Quality

Mass flowrate as a function of subcooling/quality is shown in Figure 5.2. The trends presented were consistent with the results seen for the ternary refrigerant mixture. As subcooling increased from 0°F to 20°F (11.1°C), mass flowrate increased as a second order polynomial. The figure shows that mass flowrate increased by an average of 35% as subcooling increased from 0°F to 20°F (11.1°C) for all upstream pressures tested. Refrigerant flowrate decreased as the inlet quality increased.

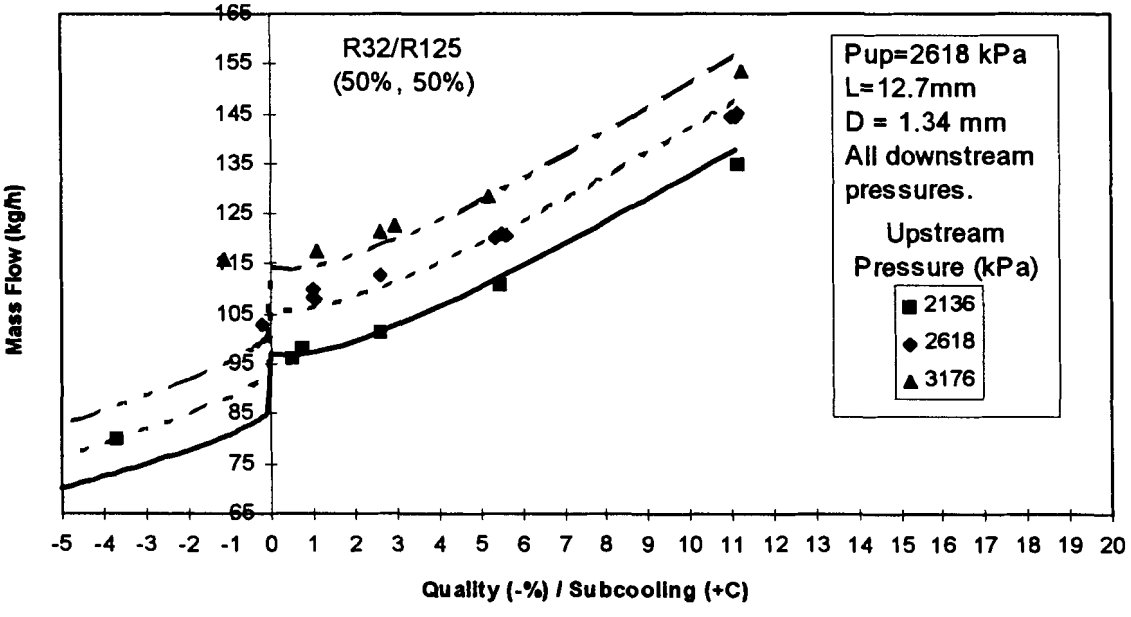

Figure 5.2: Flow dependency on subcooling/quality for all upstream pressures with length of 0.5 in (12.7 mm) and diameter of 0.0528 in (1.341 mm).

For twophase conditions at the inlet of the short tube, there was a sharp decrease in refrigerant mass flowrate as compared to the saturated conditions. Table 5.1 summarizes the change in mass flowrate for qualities between 0% and 3% for an upstream pressure of 380 psia (2618 kPa). Although the percent change in mass flowrate for twophase at the short tube entrance was approximately constant, the magnitude of the flow drop varied with diameter. This was to be expected since mass flowrate has been shown to increase in proportion to the orifice diameter raised to the power of 2.5.

Table 5.1: Mass Flowrate Change for Twophase at Orifice Inlet

Diameter, in. (mm)	Flowrate Change, lb/h (kg/h)		Difference, lb/h (kg/h)	Percent Change (%)
	0% Quality	3% Quality		
0.0432 (1.09)	139.4 (63.3)	107.2 (48.6)	32.2 (14.7)	-23.0
0.0528 (1.34)	213.9 (97.0)	165.2 (74.9)	48.7 (22.1)	-22.7
0.0674 (1.71)	375.5 (170.4)	291.4 (132.2)	84.2 (38.2)	-22.3
0.0763 (1.94)	509.11 (230.9)	396.0 (179.6)	113.1 (51.3)	-22.2

* Pup = 379.66 psia (2617.7 kPa), length = 0.5 in (12.7 mm)

Effects of Upstream Pressure

Figure 5.3 shows the variation in mass flowrate with upstream pressure at different levels of subcooling/quality. Mass flowrate tended to increase almost linearly as the upstream pressure was increased. The slope of the mass flowrate/upstream pressure line increased slightly with an increase in subcooling. The trends presented were consistent with the results seen for the ternary refrigerant mixture even though operating upstream pressures were 40% higher than those for the ternary mixture. For the figure shown, the slope increased by 14% as subcooling increased from 0°F to 20°F (11.1°C). For twophase conditions at the inlet of the short tube, mass flowrate averaged 31% lower than at a subcooling level of 20°F (11.1°C) and 7% lower than at saturated conditions. This trend was evident for all diameters tested with the additional trend of an increase in slope as diameter was increased. For example at a subcooling of 10°F (5.6°C), the slope increased from 0.219 lb/h/psia (0.686 kg/h/kPa) to 0.652 lb/h/psia (2.038 kg/h/kPa) as the diameter varied from 0.0432 in (1.09 mm) to 0.0763 in (1.94 mm). Please note the figure includes all downstream pressures.

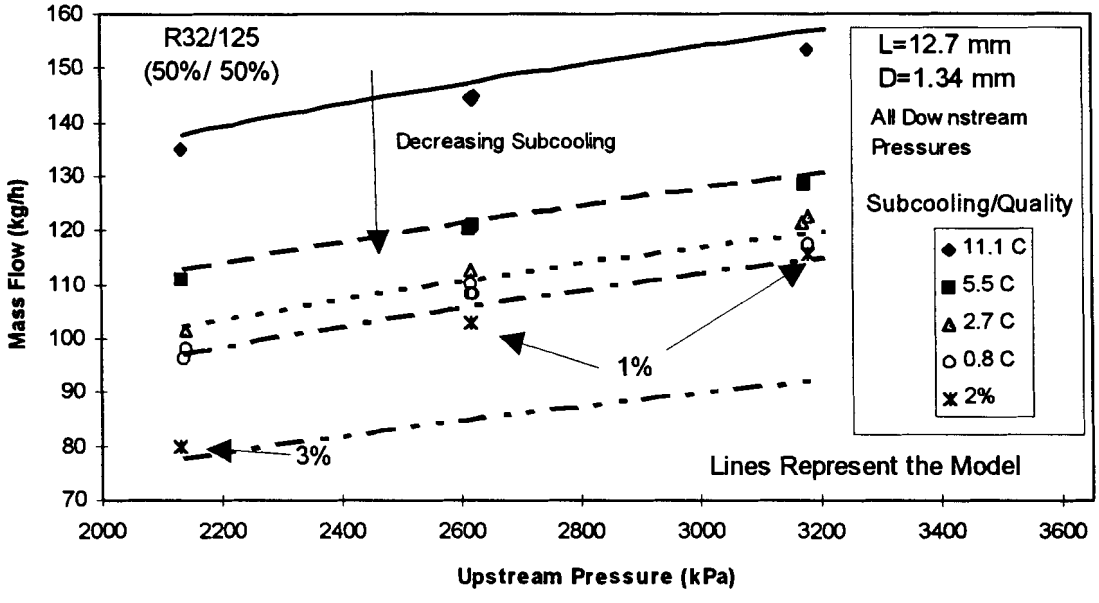

Figure 5.3: Flow dependency on upstream pressure for all subcooling/qualities and downstream pressures with length of 0.5 in (12.7 mm) and diameter of 0.0528 in (1.341 mm).

Effects of Short Tube Diameter

Figure 5.4 shows the variation in mass flowrate with orifice diameter at 20°F (11.1°C) of subcooling and all upstream pressures. While the ternary refrigerant mass flowrate tended to vary with diameter raised to the 2.2 power, the binary mass flowrate tended to vary more closely with diameter raised to the 2.5 power. Table 5.2 shows how this trend developed for several different subcooling/qualities when the data was fit to an equation of the form:

$$\dot{m} = c_1 + c_2 \cdot D^{c_3} \tag{5.1}$$

The last row in the table gives the value of the coefficient, C_3, in Equation (5.1).

Table 5.2: Variation of Mass Flowrate with Orifice Diameter

Length = 0.5 in (12.7 mm) Diameter, in (mm)	Mass Flowrate, lb/h (kg/h)		
	Subcooling/Quality		
	20°F (11.1°C)	5°F (2.7°C)	3%
0.0432 (1.09)	213.5 (96.9)	159.2 (72.2)	117.3 (53.2)
0.0528 (1.34)	325.1 (147.5)	244.5 (110.9)	180.5 (81.9)
0.0674 (1.71)	551.8 (250.3)	426.8 (193.6)	317.9 (144.2)
0.0763 (1.94)	728.4 (330.4)	575.5 (261.0)	431.5 (195.73)
c_3, coefficient	2.33	2.58	2.66

• Upstream pressure of 379.66 psia (2617.7 kPa) and all downstream pressures.

This calculation revealed the polynomial characteristics of the mass flowrate as a function of orifice diameter for the binary refrigerant. The above polynomial fits reveals the necessity of measuring the orifice diameter accurately.

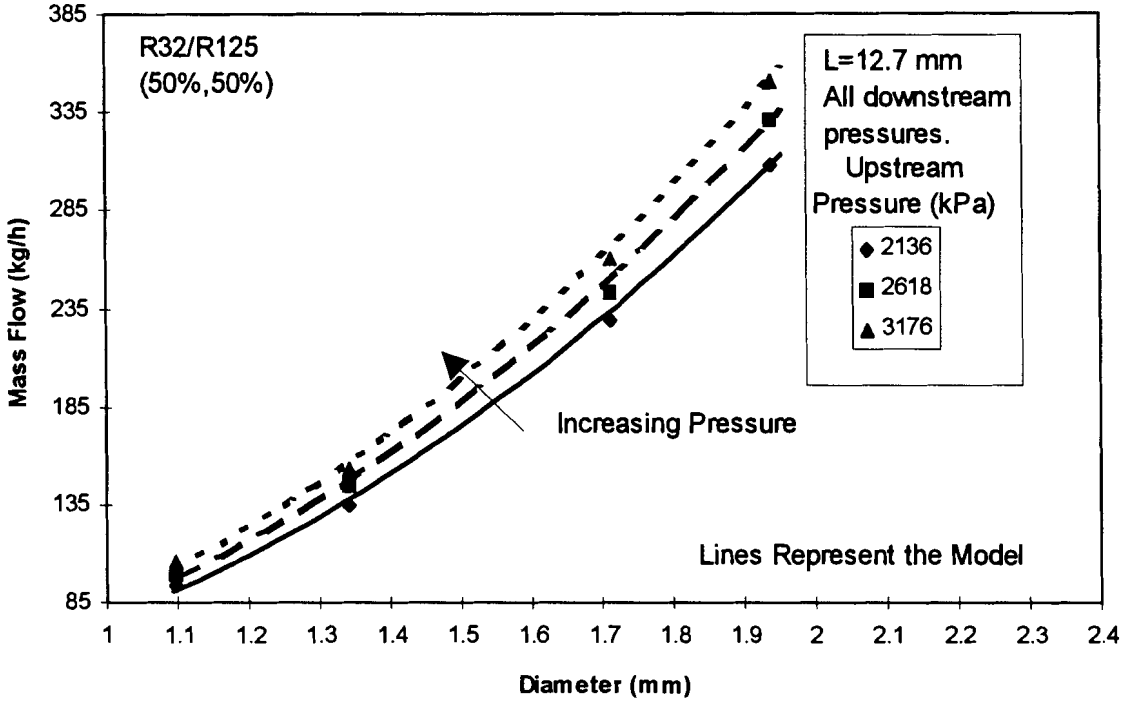

Figure 5.4: Flow dependency on short tube diameter for all upstream pressures at 20°F (11.1°C) subcooling and all downstream pressures.

Effects of Short Tube Length

Figure 5.5 shows the effects of increasing the short tube length for the given conditions. As length increased the mass flowrate of refrigerant decreased slightly. For the range of lengths being tested, the mass flowrate decreased an average of 4.5%. As subcooling decreased from 20°F (11.1°C) to 0°F, the slope of the mass flowrate versus length curve increased by 42% varying from -28.4 lb/(h in) [-0.508 kg/(h mm)] to -16.6 lb/(h in) [-0.296 kg/(h mm)]. The trends shown below were consistent with all the orifices tested.

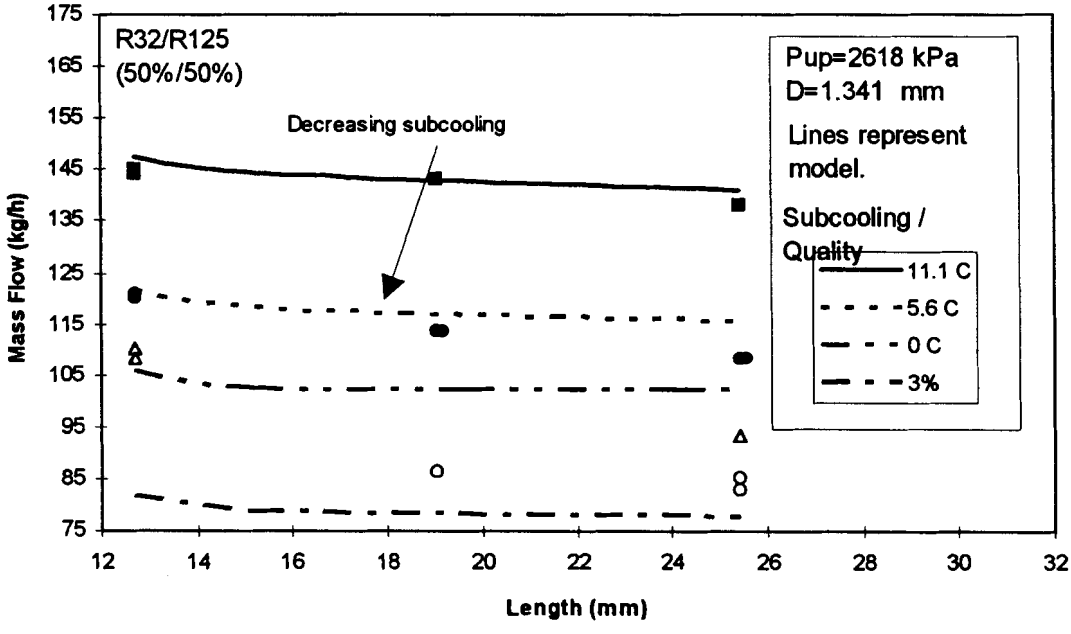

Figure 5.5: Effect of length on mass flowrate for short tube of diameter 0.0528 in (1.341 mm), upstream pressure of 380 psia (2618 kPa), and several subcoolings/qualities.

MIXTURES OF OIL AND R32/125 (50%/50%)

Tests were performed for all orifices with oil added to the pure refrigerant to more closely simulate actual operating conditions for air conditioners and heat pumps. Oil mass percentage was set at approximately 2.2%. Testing was performed at various upstream pressures and at the median downstream pressure of 132.7 psia (915 kPa). Oil concentration was determined using the methods described in chapter two (pure refrigerant method).

General Trends

Figure 5.6 shows the variation in mass flowrate ratio, m_r, as a function of oil concentration for several subcooling/qualities. The apparent scatter in the data was due to the large dependency of mass flowrate on the degree of upstream subcooling. A general trend of the form seen for the ternary refrigerant was again apparent for the binary refrigerant. At an oil concentration of 2.2% with subcoolings above 10°F (5.6°C), the refrigerant remained within 1.5% of the pure case. The mass flow ratio generally tended to decrease with decreasing subcooling. The twophase data showed an increase in mass flow ratio as quality increased from 1% to 5%. For a fixed subcooling, mass flow ratio tended to decrease as upstream pressure increased. This could be a consequence of the solubility of the oil in the refrigerant at different temperatures (Corr et al 1994). These trends were seen to apply for all orifices and upstream pressures tested.

The main emphasis of Figure 5.6 should be that oil concentrations lower than approximately 2% cause less than a 2% variation in mass flowrate as compared to the pure case. This was true of all the orifices tested. Additional data for lower oil concentrations would clarify the exact form of the mass flow ratio and oil concentration function. However, the flow trends shown seemed to agree with previous trends seen for the ternary refrigerant.

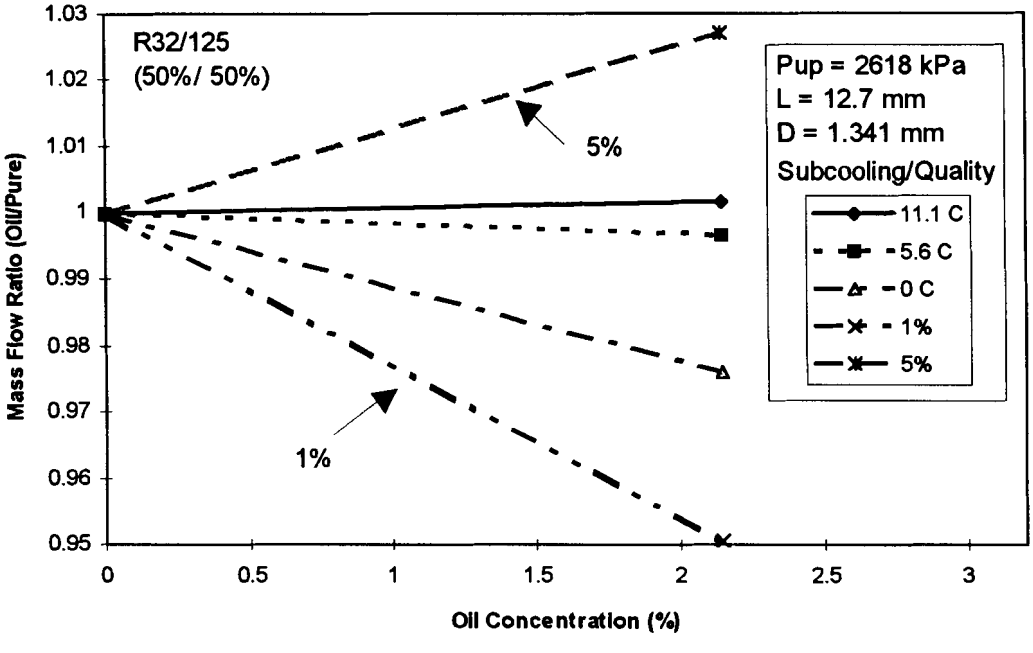

Figure 5.6: Flow dependency on oil concentration for short tube with length of 0.5 in (12.7 mm), diameter of 0.0528 in (1.341 mm), several subcooling/qualities, and upstream pressures of 380 psia (2618 kPa).

Effects of Upstream Subcooling/Quality

Figure 5.7 shows the flow dependency on upstream subcooling for the binary refrigerant mixture with 2.2% POE oil flowing through the 0.0528 in. (1.34 mm) diameter orifice. All upstream pressures were included in the figure. The mass flow ratio was calculated based upon the method introduced in chapter four.

At subcooling levels of 20°F (11.1°C), the addition of oil to the pure refrigerant caused the mass flowrate remain essentially constant as compared to the pure case. For all diameters and subcoolings, the mass flowrate for the oil refrigerant mixture remained within 5% of the pure case. As the subcooling was lowered, the mass flowrate decreased below the levels seen for the same conditions in the pure case. At subcooling levels of 10°F (5.5°C), the mass flowrate averaged 2% lower than the pure case for all diameters. This trend continued with the mass flowrate averaging 2.5% lower than the pure case at saturated upstream conditions for all diameters. In the low quality twophase region, the addition of oil decreased mass flowrate by as much as 9.5% from the pure case. As the quality increased, the mass flow ratio approached unity. Thus, for the high inlet quality region, the presence of oil did not substantially affect the mass flow.

The drop in flowrate at the lower subcooling levels for the 0.5 in (12.7 mm) orifice was consistent with results presented by Kim (1993) for mixtures of R134a and PAG oil. The binary refrigerant showed the same trends as the R134a/PAG mixture in the subcooled and twophase regions.

Effects of Upstream Pressure

The flow dependency on upstream pressure for the oil/refrigerant mixture is shown in Figure 5.8. This figure shows the trends for a 0.0674 in. (1.71 mm) diameter orifice for all subcoolings. The near horizontal nature of lines showed a weak dependence of flowrate ratio on upstream pressure. This meant that mass flowrate for the oil/refrigerant mixture tended to follow the same trends as seen for the pure case.

The main emphasis of this figure was that mass flowrate was lowered for all upstream pressures and subcoolings of 10°F (5.6°C) or less. The figure shows that mass flowrate averaged approximately 1.8% lower than the pure case for the 0.0674 in. (1.71 mm) diameter orifice at subcoolings of 10°F (5.6°C) or less. This trend was extended to all diameters with mass flowrate averaging 1% lower than the pure case for subcoolings of 10°F (5.6°C) or less.

For these oil tests, the length of the short tube was also varied. Short tubes of length 0.5 in (12.7 mm), 0.75 in (19.05 mm), and 1.0 in (25.4 mm) were tested. These orifices had diameters of 0.0528 in (1.341 mm) and 0.0674 mm (1.71 mm). At the oil concentration of 2.15%, mass flow rate remained within 1% of its value for the pure refrigerant at all lengths and for the two diameters tested. Therefore, mass flow trends were consistent with those produced by the pure refrigerant.

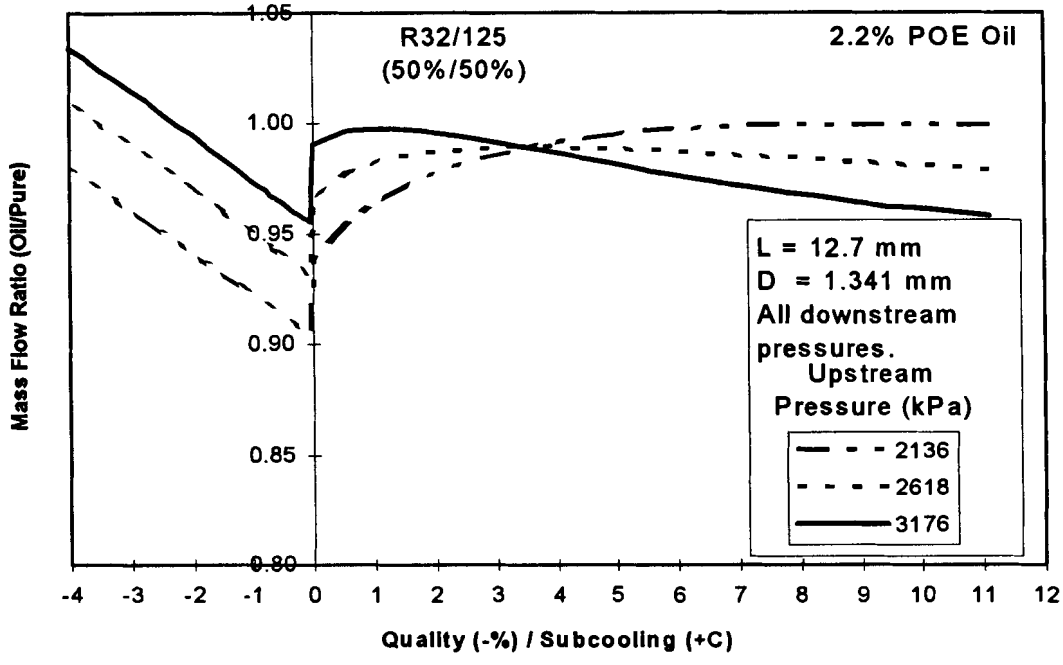

Figure 5.7: Flow dependency on upstream subcooling at all upstream pressures for the 0.0528 in (12.7 mm) diameter orifice.

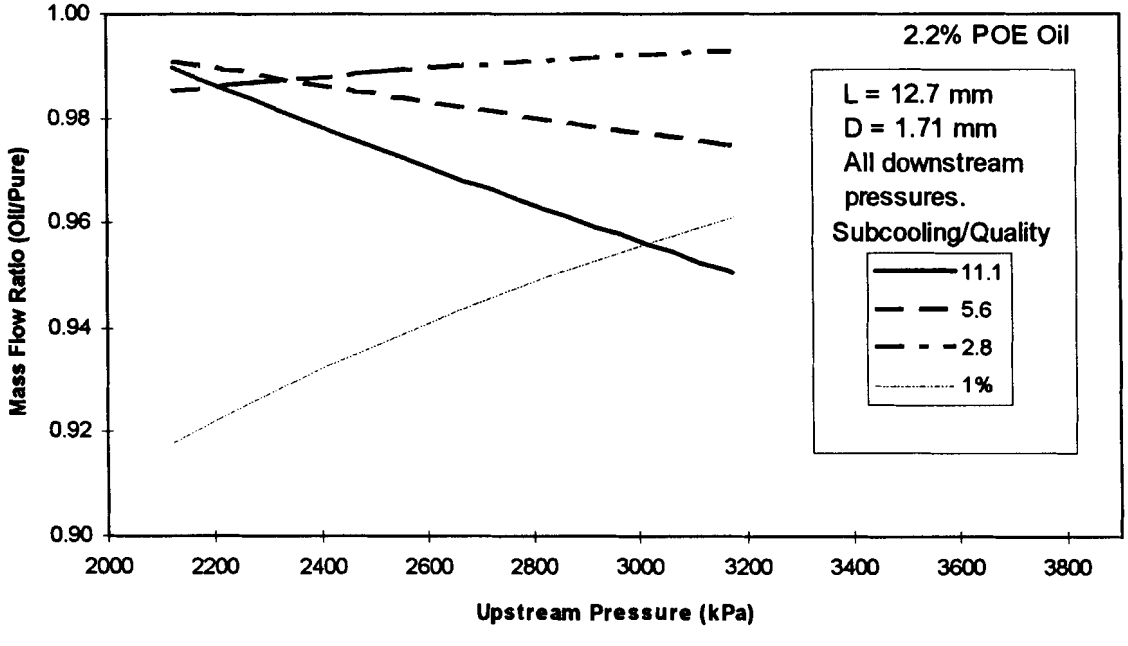

Figure 5.8: Flow dependency on upstream pressure the short tube with diameter of 0.0674 in. (1.71 mm) and length of 0.5 in (12.7 mm).

SUMMARY OF RESULTS FOR R32/125 (50%/50%)

For the high operating pressures of the binary refrigerant mixture, approximately choked flow conditions existed at all downstream pressure. Regardless of the diameter of the short tube, the mass flowrate varied by less than 1% for the range of downstream pressures tested.

As the upstream subcooling decreased, the mass flowrate of refrigerant decreased. Table 5.3 reiterates some of the data shown in Table 5.1, but also shows the trends in mass flowrate for decreasing subcooling. As subcooling decreased from 20°F (11.1°C) to 0°F, mass flowrate decreased an average of 27%. Mass flowrate increased in a polynomial fashion with increases in upstream subcooling. For twophase at the orifice inlet, the mass flowrate decreased sharply. Mass flowrate for all diameters dropped an average of 23% as quality was increased from 0% to 3%. The magnitude of the resulting decrease in mass flowrate for twophase conditions was higher for larger diameter orifices. This meant that the larger orifices tended to be more affected by twophase conditions at the entrance.

The slope of the mass flowrate/upstream pressure curve increased as upstream subcooling was increased. This trend continued for all diameter orifices. For twophase at the orifice inlet, the mass flowrate averaged 18% lower than at saturated conditions for all diameters.

The short tube diameter had a larger effect on mass flowrate for the binary refrigerant than for the ternary refrigerant. While the ternary refrigerant mass flowrate varied approximately with the square of the orifice diameter (diameter raised to the 2.2), the binary refrigerant mass flowrate tended to vary more closely with orifice diameter raised to the power of 2.5. This was true for all diameters and upstream subcooling/quality conditions.

Table 5.3: Percent Change in Mass Flowrate for a Change in Subcooling/Quality

Length of 0.5 in (12.7 mm)	Pup = 310 psia (2136 kPa)		Pup = 380 psia (2618 kPa)		Pup = 461 psia (3176 kPa)	
	Subcooling / Quality		Subcooling / Quality		Subcooling / Quality	
Diameter, in (mm)	20°F→0°F 11.1°C→0°C	0%→3%	20°F→0°F 11.1°C→0°C	0%→3%	20°F→0°F 11.1°C→0°C	0%→3%
0.0432 (1.09)	-31.5	-23.1	-28.7	-23.0	-27.4	-22.9
0.0528 (1.341)	-29.6	-22.8	-28.2	-22.7	-26.9	-22.6
0.0674 (1.71)	-27.1	-22.4	-25.8	-22.3	-24.7	-22.3
0.0763 (1.94)	-25.1	-22.2	-23.9	-22.2	-23.0	-22.1

The addition of oil to the pure refrigerant caused flow trends that were also observed in the ternary refrigerant mixture. The addition of oil below a concentration of approximately 2% would appear to only slightly affect the mass flowrate. At subcooling levels of 20°F (11.1°C), the mass flowrate change was negligible. As subcooling decreased, the decrease in mass flowrate as compared to the pure case followed a seemingly linear trend dropping by approximately 4% for all diameters tested. Increasing the length of the short tube for the oil/refrigerant mixture caused less than a 1% change in mass flowrate.

CHAPTER VI

SEMI-EMPIRICAL MODEL DEVELOPMENT

Due to complicated flow conditions and a discontinuity at the exit plane of the short tube, most previous investigators have chosen semi-empirical flow models over analytical or numerical models for refrigerant flow through short tubes. One approach to modeling twophase flow through short tubes is to start with the single-phase orifice equation and make corrections in it . This method has been used by several previous researchers (Pasqua, 1953; Davies & Daniels, 1973; Mei, 1982; and Aaron & Domanski, 1990).

The present flow model was basically derived from the single-phase orifice equation with adequate modification of a theoretical equation to satisfy the flow characteristics through short tube orifices. The developed flow model for both R32/125/134a (23/25/52) and R32/125 (50/50) covered single and twophase flow at the inlet of the short tube with consideration for oil contamination effects. This section discusses the governing equations and coefficients for the semi-empirical flow model. The detail description of theoretical equations will not be included here, but the detailed procedure can be found in the paper by Kim and O'Neal (1994a).

The single-phase orifice equation used for orifices can be derived from equations of continuity and energy with the given assumptions (ASME, 1971). The single-phase orifice equation for a single-component, single-phase substance is given as:

$$\dot{m}_s = C A_s \sqrt{2\gamma_o \rho (P_{up} - P_{down}) / (1-\beta^4)} \tag{6.1}$$

where $\dot{m}_s$ is the mass flowrate for single -phase flow and β is the ratio of orifice throat diameter to upstream tube diameter.

The total mass flow for twophase flow, $\dot{m}_{tp}$, can be related to the inlet quality, x_{up}, and single-phase mass flow rate, $\dot{m}_s$ by the following relationship (Kim and O'Neal, 1994a; Chisholm, 1967) :

$$\dot{m}_{tp} = \frac{\dot{m}_s}{(1-x_{up})\cdot(1+aY+Y^2)^{0.5}} \tag{6.2}$$

where Y is a variable that depends on the upstream quality, relative densities of the inlet vapor and liquid, and another term, F, which is a function of the polytropic ratio, n, and the pressure ratio of downstream to upstream, r. Y and F are given below:

$$Y = \frac{x_{up}}{1-x_{up}}\left(\frac{\rho_f}{\rho_g}\right)^{0.5} F \tag{6.3}$$

$$F = \left(\frac{n-1}{n}\cdot\frac{1-r}{1-r^{(n-1)/n}}\cdot\frac{1}{r^{2/n}}\right)^{0.5} \tag{6.4}$$

The variable a in Equation (6.2) depends on the cross sectional areas occupied by the liquid and vapor (Chisholm, 1967).

When an arbitrary control volume (shown by dotted line in Figure 6.1) was drawn around the short tube orifice with subcooled liquid at the inlet, it was noted that the assumption of incompressible flow for Equation (6.1) was violated due to the fact that flashing occurred inside of the short tube (Kim and O'Neal, 1993a). Once the flow flashed, there was a density change. Because choked conditions were established just after the flashing point, the flow rate was not a function of the pressure at the downstream control surface. Therefore, the downstream control surface was reset to the inlet section before flashing occurred (shown by continuous line in Figure 6.1).

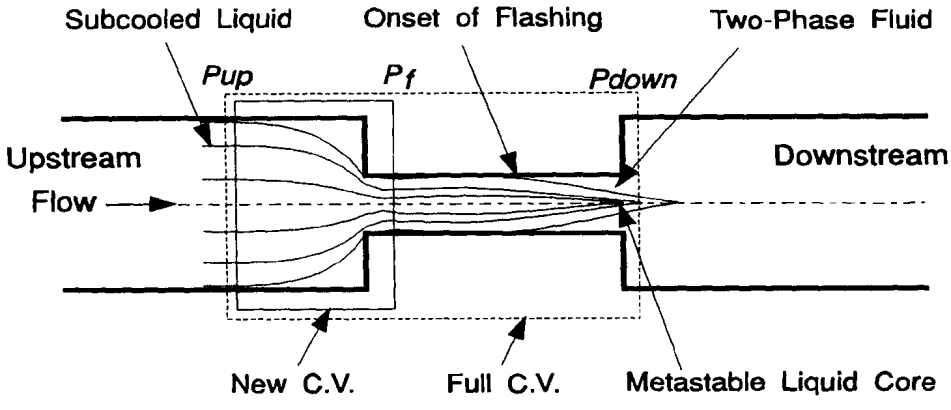

Figure 6.1: Control Volume of the Mass Flow Model.

It was observed that the measured pressure at the inlet section of the short tube was lower than P_{sat} (Kim, 1993). However, due to the existence of metastable liquid flow at the inlet section of the tube, the temperature change anticipated from the pressure dip near the inlet could be small within the new control volume. Therefore, the change of the liquid density across the control volume may be assumed to be negligible because of small temperature differences. Thus, the assumption of incompressible flow was approximately satisfied by moving the downstream control surface.

Once the assumptions were examined with the new control volume, Equations (6.1) and (6.2) had to be modified to satisfy both the flow characteristics through short tubes and flow conditions within the new control volume. After dropping the term $(1-\beta^4)$ from Equation (6.1) due to small values of β^4 compared with unity (for current study, $0.1 < \beta < 0.2$), a mass flow model for both single and twophase flow was derived by combining Equations (6.1) and (6.2):

$$\dot{m} = C \cdot C_{tp} \cdot A_s \sqrt{2\gamma_c \rho_f (P_{up} - P_{down})} \tag{6.5}$$

where,

$$C_{tp} = \left[\left(1 - x_{up}\right) \cdot \left(1 + aY + Y^2\right)^{0.5} \right]^{-1} \tag{6.6}$$

It should be noted that for single-phase flow entering the short tube, the mass flow rate, $\dot{m}_{tp}$ was equal to $\dot{m}_s$ (Equation (6.1)) because C_{tp} was unity. For twophase flow entering the short tube, $\dot{m}$ and $\dot{m}_{tp}$ (Equation (6.2)) were identical.

To satisfy the pressure condition at the downstream control surface, P_f, which was the pressure before the flashing occurred, was applied instead of P_{down}. The adjusted downstream pressure, P_f, covered the assumption of incompressible flow and choked flow conditions. The single-phase flow models were typically correlated by modifying downstream pressure and the orifice constant. In this study, the orifice constant, C, was set equal to unity and P_f was correlated with the experimental data. Due to the limited data for oil contamination, a correction factor for oil contamination was not included in the present model. New coefficients for the oil/refrigerant mixtures were calculated instead. Further testing of these refrigerants at various concentrations of oil would be needed to properly correlated mass flowrate with oil concentration. The final form of the model was given by:

$$\dot{m} = C_{tp} A_s \sqrt{2 \gamma_c \rho (P_{up} - P_f)} \tag{6.7}$$

where,

A_s = short tube throat area, in^2 (m^2)
C_{tp} = correction factor for twophase quality (Equation (6.9))
$\dot{m}$ = mass flowrate, lb/h (kg/h)
P_f = adjusted downstream pressure, psia (kPa) (Equation (6.8))
P_{up} = upstream (condenser) pressure, psia (kPa)
ρ = density of upstream fluid entering short tubes, lb/ft^3 (kg/m^3)
(for twophase entering the short tube, ρ equals to ρ_f)

The variables, P_f, and C_{tp}, in Equation (6.7) were correlated with respect to a normalized form of each of the operating parameters and short tube diameter. The use of a normalized form allowed the applicability of SI and English units. The Equation (6.7) was formed to cover single and twophase flow at the inlet of the short tube without considering oil

mixture effects. It should also be noted that for subcooled liquid entering the short tube, C_{tp} was unity because x_{up} in Equation (6.9) was set equal to zero.

After deciding basic normalized parameters included in each correction factor, a correlation between correction factor and normalized parameters was determined using a non-linear regression technique along with the experimental data. All coefficients included in the flow model are given at Table 6.1.

Based on the all measured data for pure refrigerants, the adjusted downstream pressure, P_f, was correlated with inlet subcooling, upstream pressure, downstream pressure, short tube length, and short tube diameter. The liquid saturation pressure, P_{sat}, was used as a reference value for P_f, because flashing occurred when the pressure was near P_{sat}.

$$P_f = P_{sat}\left[\begin{array}{c} b_1 + b_2 \cdot PRA^{b_3} \cdot LD^{b_4} \cdot SUBC^{b_5} + b_6 \cdot PRA^{b_7} \\ + b_8 \cdot exp(b_9 \cdot DR \cdot LD^{b_{10}}) + b_{11} \cdot EVAP \end{array}\right] \tag{6.8}$$

where,

DR = D/D_{ref}

$EVAP$ = $(P_c - P_{down})/P_c$ (P is in absolute pressures)

LD = (L / D)

PRA = P_{up}/P_c (P is in absolute pressures)

$SUBC$ = $(T_{sat} - T_{up})/T_c$ (T is in absolute temperatures)

D = short tube diameter, in. (mm)

D_{ref} = reference short tube diameter, 0.060 in. (1.524 mm)

P_c = critical pressure for a given refrigerant, psia (kPa)

P_{down} = downstream (evaporator) pressure, psia (kPa)

P_{sat} = saturated liquid pressure corresponding to upstream temperature, psia (kPa)

T_c = critical temperature for a given refrigerant, °R (K)

Table 6.1: Coefficients of Correction Factors in the Flow Model

Equations	Coefficients	R32/125/134a (23/25/52)		R32/125 (50/50)	
		Pure	1% Oil	Pure	2.2% Oil
Eq (6.8)	b_1	0.963034325	0.980538238	0.874805831	1.050104183
	b_2	4.286408416	4.957604391	3.131470913	6.305986547
	b_3	-0.278235435	-0.309919995	-0.214726407	0.099138818
	b_4	-0.043090943	-0.116219951	0.083394737	-0.045626106
	b_5	0.916226528	0.906610038	0.901559277	0.958459297
	b_6	0.071794702	0.227476573	-0.020574536	-0.254071783
	b_7	0.499098698	0.186773583	0.944446846	0.137198955
	b_8	-0.208417565	-0.398196082	-0.418400083	-0.276516186
	b_9	-0.034680678	-0.030711793	-0.025322802	-0.014589768
	b_{10}	1.844061084	1.587754176	2.33507746	2.5121908
	b_{11}	-0.091235910	-0.134132834	0.068890172	0.13087558
Eq (6.9)	a_1	-4.45974577	-4.349745770	3.693038038	1.427618112
	a_2	10.69467130	10.454571210	0.120175996	0.530751112
	a_3	-0.55303036	-0.663120121	0.194241638	-0.365456266
	a_4	0.39429366	0.323273661	0.022577667	0.018669938

Constants	Unit	R32/125/134a (23/25/52)	R32/125 (50/50)
P_c	SI	4619.14 kPa	4949.65 kPa
	English	669.95 psia	717.886 psia
T_c	SI	359.89 K	345.65 K
	English	647.80 °R	622.17°R
γ_c	SI	1.2960×10^{10}	1.2960×10^{10}
	English	2.8953×10^{6}	2.8953×10^{6}

Upstream pressure, P_{up}, was considered in the updated model (Equation. (6.7)), but it did not adequately account for the observed slope change for flow rate with respect to upstream pressure and subcooling. Therefore, the effects of the upstream subcooling were correlated with the normalized subcooling, $(T_{sat}-T_{up})/T_c$ and normalized upstream pressure, P_{up}/P_c.. Because the cross sectional area of the short tube, A_s, in Equation (6.7) did not fully correlate diameter effects on flow rate, normalized form of diameter, DR, was included in the correction of the adjusted downstream pressure, P_f.. Due to non-ideal choking that occurs in orifices, the slight mass flow dependency on downstream pressure was considered using the normalized downstream pressure, $(P_c-P_{down})/P_c$..

Because the twophase correction factor, C_{tp}, defined by Equation (6.6) did not include the effects of short tube geometry and boundary conditions at the downstream control surface, some modifications were required. First, the F in Equation (6.4) was set equal to unity because of the difficulty in evaluation of pressure ratio, r, within the new control volume. However, the effects of compressibility for vapor (the physical meaning in the value of F) was considered by modifying inlet quality, x_{up} (coefficients a_1 and a_2 in Equation (6.9)). Second, the correlation between the single-phase flow rate and liquid flow rate during twophase flow was modified by including the effects of a short tube diameter. The single-phase mass flow, $\dot{m}_s$, was calculated at zero subcooling to obtain the continuity between the single and twophase flow rate. Thus, after setting $SUBC$=0 while keeping the coefficients of P_f constant, the coefficients of C_{tp} were determined from the experimental data for twophase entering the short tube.

$$C_{tp} = \frac{1}{(1+a_1 \cdot x_{up})(1+a_2 \cdot LD^{a_3} \cdot Y^{a_4 Ln(LD)})} \tag{6.9}$$

where

$$Y = \frac{x_{up}}{1-x_{up}} \cdot \left(\frac{\rho_f}{\rho_g}\right)^{0.5} \tag{6.10}$$

The ρ_f and ρ_g in the Equation (6.10) is the saturated liquid and saturated vapor density, respectively, at a given upstream pressure which is equal to saturation pressure, P_{sat}, for twophase entering the short tube.

The presence of oil had a stronger effect on mass flowrate at low subcooling levels than at high subcooling levels. The effects of the oil were partially dependent on upstream subcooling and upstream pressure (Chapter IV and V). If more data was taken for several more oil concentrations, a correction factor for oil concentration, C_o could be included in equation 6.7. However, due to limited data for mass flow at different oil concentrations, the present model only includes flow equation for the specific oil concentrations tested.

Using Equation (6.7) through (6.10), the mass flow rate at a given operating condition and short tube geometry can be predicted. When applying the above equations, it should be understood that the application of the flow model has a limited range due to the limited range of the experimental data (Table 6.2). To apply the flow model successfully, some attention is required in the following: (1) temperature and pressure are in their absolute values, and area has units of in^2 (m^2), (2) x_{up} should be set equal to zero (C_{tp}=1) for calculation of single-phase mass flow rate, (3) *SUBC* should be set equal to zero for calculation of twophase mass flow rate, and (4) the oil model does not cover every geometry included in the pure tests with twophase flow at the inlet of the short tube.

Table 6.2: Limitations on the Application of the Flow Model

Refrigerants	Parameter	Minimum	Maximum
R32/125/134a (23/25/52)	L	0.5 in (12.70 mm)	1.0 in (25.40 mm)
	D	0.0431 in (1.09 mm)	0.0763 in (1.94 mm))
	P_{up}	221 psia (1524 kPa)	329 psia (2271 kPa)
	P_{down}	78 psia (483 kPa)	P_{sat}
	Subcooling	0°F (0°C)	20°F (11.1°C)
	Quality	0 %	5 %
	Oil Conc.	0 %	1.0 %
R32/125 (50/50)	L	0.5 in (12.70 mm)	1.0 in (25.40 mm)
	D	0.0431 in (1.09 mm)	0.0763 in (1.94 mm)
	P_{up}	309 psia (1751 kPa)	461 psia (3176 kPa)
	P_{down}	111 psia (769 kPa)	P_{sat}
	Subcooling	0°F (0°C)	20°F (11.1°C)
	Quality	0 %	5 %
	Oil Conc	0 %	2.2 %

GOODNESS OF FIT

The detail comparison of the present flow model with the experimental data is included in the Appendix A. Generally the prediction of mass flowrate fit the experimental data well for a wide operating range. An absolute value percent difference as defined by the following equation was used to determine the goodness of fit for each model.

$$P_{diff} = ABS\left(\frac{calculated - actual}{actual} * 100\%\right) \tag{6.11}$$

Table 6.3 compares the model with the experimental data over the entire range of geometries and conditions tested. For the pure ternary mixture (AC9000) with both single phase at the

Table 6.3: Overall Goodness of Fit for Mass Flow Model Using 95% of the Data

	R32/125/134a (23/25/52)		R32/125 (50/50)	
Absolute Value Percent Difference	Pure	Oil	Pure	Oil
Mean	2.814	1.629	1.999	1.882
Standard Deviation	2.050	1.174	1.904	1.568
Maximum	8.420	4.145	9.394	8.296

inlet of the short tube, approximately ninety-five percent of the measured data were within ± 3% of the model's prediction (the model predicted the results with a standard deviation of 2.05%). The maximum difference between the measured data and the model's prediction was within ±10%. For the pure binary mixture (AZ20) with single phase flow at the inlet of the short tube, the predicted mass flowrate was within ±2.6% of the measured flow rates, and ninety-five percent of the experimental data were within ±2% of the model's prediction (the model predicted the results with a standard deviation of 3.6%). We hypothesize that the accuracy of the model for the ternary mixture (AC9000) was lower than the binary mixture (AZ20), due to composition change in the ternary mixture as it vaporized. The small difference between the model's prediction and experimental data could also be attributable to uncertainties in measurements such as mass flowrate.

The goodness of fit of the current model can be explored further by breaking the amount of error into groups based upon length and diameter. Tables 6.4 and 6.5 show the agreement of the model to all of the experimental data for the various lengths and diameters of short tubes. Again please note that all of the experimental data is included in the quantities presented in Tables 6.4 and 6.5.

Table 6.4: Pure Single Phase Model Comparison Based Upon Short Tube Length

	L = 0.5 in (12.7 mm)		L = 0.75 in (19.05 mm)		L = 1.0 in (25.4 mm)	
P_{diff}	Ternary	Binary	Ternary	Binary	Ternary	Binary
Mean	2.94	1.42	2.49	1.50	4.86	7.34
Standard Deviation	2.92	0.98	1.79	1.57	2.78	5.82
Maximum	18.15	4.08	7.65	6.47	10.30	22.70

* All values are absolute value percent differences between the model and experimental data.

Table 6.5: Pure Single Phase Model Comparison Based Upon Short Tube Diameter

Diameter ⇒	0.0432 in (1.09 mm)		0.0528 in (1.34 mm)		0.0674 in (1.71 mm)		0.0763 in (1.94 mm)	
P_{diff}	Ternary	Binary	Ternary	Binary	Ternary	Binary	Ternary	Binary
Mean	2.78	4.20	3.59	2.29	2.73	2.54	3.02	1.33
Standard Deviation	2.45	6.16	2.24	2.30	2.83	2.15	4.04	1.32
Maximum	10.30	22.70	11.95	9.39	16.15	7.65	18.15	4.73

* All values are absolute value percent differences between the model and experimental data.

In Table 6.4 we can see that the short tubes with lengths of 1.0 in (25.4 mm) produced the highest absolute value percent difference for mass flowrate when compared to the model. These larger deviations from the model were generally caused by one short tube which had a length of 1.0 in (25.4 mm) and diameter of 0.0431 in (1.09 mm). The maximum deviation of 22% occurred with the binary refrigerant and averaged 17.6% for this short tube. Close examination of this orifice showed no rough internal features or obvious geometric irregularities. This same orifice was modeled well for the ternary refrigerant. It was hypothesized that flow conditions within the orifice had changed due to the higher operating pressures of the binary refrigerant and the large length to diameter ratio of this orifice (23.2).

For twophase flow at the inlet of the short tube, the mass flow model did not predict flowrate as well. For the ternary refrigerant mixture the model predicted flowrate to within ±15% for all pure refrigerants and oil/refrigerant mixtures. Twophase conditions for the binary refrigerant did not show the same rapid decrease in flowrate as seen with the ternary refrigerant. This would be expected since the binary refrigerant operates at pressures which averaged 40% higher than those seen by the ternary refrigerant. The limited range of twophase data prevented the development of a good fit for all flow conditions and geometries. The absolute value percent difference for the pure case averaged 10% with a standard deviation of 7%. This also applied to the oil/refrigerant mixtures with an average absolute value percent difference of 9%. This lack of good fit could possibly be due to the uncertainty in measuring quality (±4% is the uncertainty for quality calculations).

For both refrigerants (AC9000 and AZ20) with oil, the model was a better fit due to the limited geometries tested. With the ternary refrigerant only 0.5 in (12.7 mm) orifices with diameters of 0.0528 in (1.34 mm) and 0.0676 in (1.72 mm) were tested. This limited range of experimental data was much easier to fit. Approximately ninety-five percent of the single phase data were within ±2% of the model's prediction (the oil/refrigerant models for AC9000 and AZ20 were fit the experimental results with a standard deviation of 1.3% and 2.7%, respectively). Due to the limited data range for oil concentration, the application of the model to higher oil concentrations should be used with caution. Because oil did not have any significant effect on flow rate at low oil concentration region (less than 2%), the use of pure refrigerant flow model is strongly recommended for oil concentrations ranging from 0% to 2%. The maximum error occurred from using the pure refrigerant model in the low oil concentration range should be less than ±5% of the measured mass flow.

CHAPTER VII

SUMMARY AND RECOMMENDATIONS

To develop an acceptable flow model, an experimental investigation was performed. The refrigerants investigated were those considered R22 replacements: R32/125/134a (23%/25%/52%) and R32/125 (50%/50%). A series of tests for both refrigerants were performed to generate data at varying operating conditions with twelve short tubes. The tests included both single and twophase flow conditions at the inlet of the short tube with different oil concentrations. Experimental data were presented as a function of major operating parameters and short tube diameter. Based on test results and analysis, a mass flow model was developed.

Short tube orifices of length 0.5 in (12.70 mm) to 1.0 in (25.4 mm) and diameters ranging from 0.0431 in (1.09 mm) to 0.0763 in (1.94 mm) were tested for R32/125/134a (23%/25%/52%) and R32/125 (50%/50%) at selected testing conditions found in heat pump or air-conditioner applications. The general trends observed in both refrigerants were consistent with the previous results for R22 (Kim and O'Neal, 1993a; Aaron and Domanski, 1990). At the same condensing temperature conditions, the mass flowrate of the ternary mixture varied by approximately ±5% as compared to R22 while the binary refrigerant flowrate averaged 15% higher than that for R22 due to its higher operating pressures (Table 7.1). The maximum percent difference in Table 7.1 occurred at high levels of subcooling and large qualities. Generally, flow trends of both refrigerants were also quite similar to each other even though mass flow rate for the binary mixture (AZ20) was approximately 6 to 15% higher than that for the ternary mixture (AC9000). The test results for both refrigerants showed the mass flow rate was strongly dependent on upstream conditions, but slightly dependent on downstream conditions.

Table 7.1: Comparison of the Mass Flowrate for a Short Tube with L=0.5 in (12.7 mm) and D=0.0528 in (1.34 mm).

Sat. Liq. Temp., °F (°C)	Subcooling / Quality °F (°C)	Refrigerant Flow, lb/h (kg/h)			% Differences	
		R22	R32/125/134a (23%/25%/52%)	R32/125 (50%/50%)	R32/125/134a (23%/25%/52 %)	R32/125 (50%/50%)
95 (35)	20 (11.1)	259 (117)	264 (120)	304 (138)	1.9	17.4
$P_{Sat\ Liq}$:	10 (5.6)	224 (102)	225 (102)	249 (113)	0.4	11.2
R22 : 196 psia (1351 kPa)	5 (2.8)	211 (96)	211 (96)	225 (102)	0.0	6.6
Ternary : 221 psia (1524 kPa)	0	201 (91)	210 (95)	214 (97)	4.5	6.5
Binary : 309 psia (2130 kPa)	5%	138 (63)	152 (69)	154 (70)	10.1	11.6
110 (43.3)	20 (11.1)	281 (127)	289 (131)	325 (147)	2.9	15.7
$P_{Sat\ Liq}$:	10 (5.6)	242 (110)	247 (112)	268 (122)	2.1	10.7
R22 : 241 psia (1662 kPa)	5 (2.8)	226 (103)	230 (104)	245 (111)	1.8	8.4
Ternary : 271 psia (1868 kPa)	0	212 (96)	225 (102)	234 (106)	6.1	10.4
Binary : 379 psia (2613 kPa)	5%	157 (71)	170 (77)	169 (77)	8.3	7.6

* Percent difference = (Refrigerant Mixtures - R22)/R22.

The major factor affecting the flow rate was upstream conditions. For both subcooled liquid and twophase flow entering a short tube, the mass flow rate was directly proportional to upstream pressure. The increase in mass flowrate with upstream pressure was accelerated for high levels of upstream subcooling. The refrigerant flow rate increased in a polynomial fashion with increases in upstream subcooling. The mass flow continued dropping inside the saturation region as the quality increased.

The mass flow rate was extremely sensitive to changes in short tube diameter. The binary mixture (AZ20) showed more effects of short tube diameter on flowrate than the ternary mixture (AC9000). While the ternary refrigerant mass flowrate in the subcooling region varied approximately with the square of the orifice diameter, the binary refrigerant mass flowrate tended to vary more closely with diameter raised to the 2.6 power. The effects of diameter varied as a function of upstream subcooling and quality.

The effects of oil contamination on the flow through short tubes were studied by comparing test results for oil contaminated refrigerants with pure refrigerants (mass flow ratio m_R). The presence of oil below a concentration of approximately 2% would appear to only slightly affect the mass flowrate (less than 5%). For both refrigerants at high levels of subcooling (beyond 10°F (5.6°C)), the addition of oil varied flowrate from the pure case by ± 5%. As subcooling decreased, the decrease in mass flow as compared to the pure case followed a linear trend.

To predict the mass flow rate, the semi-empirical models for both single and twophase flow at the inlet of the short tubes were developed by empirically correcting the modified orifice equation as a function of normalized forms of operating conditions. Due to the limited range of oil concentrations tested, new coefficients were calculated for each oil concentration tested. It was found that the semi-empirical flow model estimates were in good agreement with laboratory results for both single and twophase flow entering the short tubes.

The tests for the effects of oil concentration was performed over a limited range of test conditions and short tube diameters with one lubricant: RL 32S POE. The polyol ester lubricant was of a single viscosity, 32 centistokes. Oils of higher viscosity could produce different results from what was seen here. Also the miscibility of the oil and refrigerant were not factored into model development. Although this oil was reported to be miscible with the refrigerants under the test conditions, other oils may not show this same behavior. Further study would be required to characterize the effects of oil concentration with short tube geometry and test conditions.

It was earlier noted that the limitations on the application of the semi-empirical flow model were imposed by the range of the experimental data. Therefore, a more comprehensive semi-empirical model may need to be developed to obtain a wider applicability.

REFERENCES

Aaron, A.A., and Domanski, P.A. 1990. "Experimentation, analysis, and correlation of refrigerant-22 flow through short tube restrictors." *ASHRAE Transactions*, Vol. 96, Part 1, pp. 729-742.

ASHRAE. 1984. *ANSI/ASHRAE Standard 41.4-1984, Standard method for measurement of proportion of oil in liquid refrigerant.* Atlanta: American Society of Heating, Refrigerating, and Air-Conditioning Engineers, Inc.

ASME. 1971. *Fluid meters - their theory and application,* sixth edition. New York: The American Society of Mechanical Engineers, Inc.

Chisholm, D. 1967. "Flow of compressible twophase mixtures through throttling devices." *Chemical and Process Engineering*, Vol. 48, pp. 342-350.

Corr, Stuart; Murphy, F. Thomas, and Wilkinson, Stuart. 1994. "Composition shifts of zeotropic HFC refrigerants in service", *ASHRAE Transactions,* Vol 100, Pt.2.

Davies, D., and Daniels, T.C. 1973. "Single and twophase flow of dichlorodifluoromethane, (R-12), through sharp-edged orifice." *ASHRAE Transactions*, Vol. 79, Part 1, pp. 109-123.

Krakow, K.I., and Lin, S. 1988. "Refrigerant flow through orifices." *ASHRAE Transactions*, Vol. 94, Part 1, pp. 484-506.

Kim, Y., 1993. "Twophase flow of HCFC-22 and HFC-134a through short tube orifices." Ph.D. Dissertation, Texas A&M University, Texas.

Kim, Y. and O'Neal, D.L., 1993a. "Twophase flow of refrigerant-22 through short tube orifices." *ASHRAE Transactions,* Vol. 100, Part 1.

Kim, Y. and O'Neal, D.L., 1993b. "An experimental study of twophase flow of HFC-134a through short tube orifices." Heat Pump and Refrigeration System Design, Analysis, and Applications, AES Vol 29, ASME Winter Annual Meeting New Orleans.

Kim, Y. and O'Neal, D.L., 1994a. "A semi-empirical model of twophase flow of refrigerant-134a through short tube orifices." Accepted for publication in *Experimental Thermal and Fluid Science*, Vol 7, No. 8.

Kim, Y. and O'Neal, D.L., 1994b. "The effect of oil on the twophase critical flow of refrigerant 134a through short tube orifices." *International Journal of Heat and Mass Transfer*, Vol. 37, No. 9, pp. 1377-86.

Kline, S.J., and McClintock, F.A. 1953. "Describing uncertainties in single sample experiments." *Mechanical Engineering*, Vol. 75, pp. 3-8.

McLinden, M.O., and Gallagher, J.S., et al. 1990. "Measurement and formulation of the thermodynamic properties of refrigerants 134a and 123." *ASHRAE Transactions*, Vol. 96, Part 1, pp. 263-283.

Mei, V.C. 1982. "Short tube refrigerant restrictors." *ASHRAE Transactions*, Vol. 88, Part 2, pp. 157-168.

Pasqua, P.F. 1953. "Metastable flow of Freon-12." *Refri. Eng.*, Vol. 61, pp. 1084A-1088.

Tree, D.R. 1970. "Liquid flow measurements special considerations for liquid refrigerants." Symposium on Flow Measurement, ASHRAE.

Zaloudek, R.R. 1963. "The critical flow of hot water through short tube." HW-77594, Hanford Lab., Richland, Washington.

APPENDIX A

MODEL COMPARISON WITH EXPERIMENTAL DATA

The semi-empirical flow model was developed to predict the mass flowrate through short tubes with a given sets of conditions. The flow model was formed to cover both single and twophase flow at the inlet of the short tube with consideration for the effects of oil concentration. This appendix presents the experimental data with the predicted mass flowrate using the mass flow model developed in chapter six. It consists of four sections for each refrigerants either with or without oil:

A.1. Pure R32/125/134 (23%/25%/52%) (AC9000)
A.2. Pure R32/125 (50%/50%) (AZ20)
A.3. Mixtures of oil and R32/125/134a (23%/25%/52%)
A.4. Mixtures of oil and R32/125 (50%/50%).

The variables used in each column of the table are defined as:

L = short tube length (inch)
D = short tube diameter (inch)
Pup = upstream (condensing) pressure (psia)
Pdown = downstream (evaporating) pressure (psia)
Tsub = upstream subcooling (°F)or quality (%)
(negative value indicates quality)
Mact = measured mass flowrate (lb/min)
Mcalc = predicted flowrate using the mass flow model (lb/min)
(Mcalc - Mact) /Mact = percent difference between the predicted and measured mass flowrate (%)

A1. Pure R32/125/134a (23%/ 25%/ 52%) by mass

PUP	PDOWN	TSUB	L	D	MACT	MCALC	%DIFF
221.57	77.94	20.205	0.5	0.0432	3.123	2.9908	-4.2336
221.41	92.05	19.958	0.5	0.0432	3.098	2.9643	-4.3142
220.22	91.89	9.811	0.5	0.0432	2.478	2.4768	-0.0486
220.81	91.87	4.792	0.5	0.0432	2.292	2.2944	0.1039
221.94	94.04	0.469	0.5	0.0432	2.186	2.22	1.5541
219.71	93.26	-0.275	0.5	0.0432	2.157	1.9547	-9.3783
221.44	94.01	-0.396	0.5	0.0432	2.175	2.0459	-5.934
222.02	93.02	-0.981	0.5	0.0432	1.986	1.7773	10.507
220.85	94.35	-3.063	0.5	0.0432	1.696	1.9901	17.3409
271.45	110.32	19.971	0.5	0.0432	3.261	3.1365	-3.8181
271.86	93.39	19.909	0.5	0.0432	3.3	3.1524	-4.4721
270.73	78.73	19.732	0.5	0.0432	3.253	3.1549	-3.0163
271.4	78.93	10.369	0.5	0.0432	2.688	2.6856	-0.091
271.21	111.81	10.188	0.5	0.0432	2.65	2.6303	-0.7451
271.86	93.29	10.149	0.5	0.0432	2.683	2.6564	-0.9926
271.35	78.58	9.497	0.5	0.0432	2.631	2.6471	0.6106
269.89	94.4	3.945	0.5	0.0432	2.421	2.4105	-0.4348
271.22	110.59	2.063	0.5	0.0432	2.345	2.3413	-0.1575
269.63	110.33	1.305	0.5	0.0432	2.291	2.3272	1.5802
271.21	80.29	1.105	0.5	0.0432	2.292	2.3822	3.9345
270.67	110.77	0.649	0.5	0.0432	2.227	2.325	4.4022
272.24	93.86	-0.131	0.5	0.0432	2.253	2.2951	1.8686
272.05	93.24	-0.227	0.5	0.0432	2.182	2.1456	-1.6688
271.23	92.78	-1.22	0.5	0.0432	2.008	2.0729	3.2338
272.18	92.15	-4.1	0.5	0.0432	1.894	2.1613	14.112
328.46	93.37	19.969	0.5	0.0432	3.507	3.3286	-5.0862
328.63	92.86	9.921	0.5	0.0432	2.866	2.7911	-2.6135
328.22	92.08	4.435	0.5	0.0432	2.66	2.5628	-3.6529
329.21	92.89	2.422	0.5	0.0432	2.544	2.5068	-1.4622
327.83	94.88	1.825	0.5	0.0432	2.525	2.4885	-1.446
328.97	92.89	1.425	0.5	0.0432	2.517	2.4885	-1.1315
327.23	93.97	-0.072	0.5	0.0432	2.404	2.4431	1.6261
329.18	92.92	-4.733	0.5	0.0432	2.087	2.3885	14.4474
221.8	93.15	20.544	0.5	0.0528	4.369	4.5456	4.0418
221.78	92.4	10.376	0.5	0.0528	3.651	3.8521	5.509
221.59	92.2	4.998	0.5	0.0528	3.522	3.5738	1.4717
221.23	94.02	1.901	0.5	0.0528	3.424	3.4733	1.4412
220.89	93.6	-1.721	0.5	0.0528	2.698	3.1043	15.0608
270.92	92.62	20.38	0.5	0.0528	4.704	4.8269	2.6117
271.43	93.15	20.352	0.5	0.0528	4.641	4.8258	3.9818
271.21	93.35	20.097	0.5	0.0528	4.684	4.8045	2.5723
271.17	110.43	19.834	0.5	0.0528	4.603	4.7573	3.3513
270.68	93.89	19.562	0.5	0.0528	4.575	4.7601	4.0468
272.06	94.26	10.199	0.5	0.0528	3.878	4.0948	5.5916
270.6	110.85	9.854	0.5	0.0528	3.852	4.0323	4.6811
271.46	94.28	9.849	0.5	0.0528	3.86	4.0699	5.4389
271.61	111.8	5.042	0.5	0.0528	3.679	3.7673	2.3991
271.2	94.96	4.969	0.5	0.0528	3.62	3.8018	5.0209
271.58	110.61	4.769	0.5	0.0528	3.665	3.7578	2.531
271.6	95.13	2.086	0.5	0.0528	3.552	3.7044	4.2905
271.83	94	1.682	0.5	0.0528	3.577	3.7001	3.4423

270.73	112.08	1.568	0.5	0.0528	3.519	3.6487	3.6858
270.97	94.15	1.305	0.5	0.0528	3.522	3.6912	4.8042
271.05	94.27	0.955	0.5	0.0528	3.501	3.6884	5.3531
271.04	92.09	-2.895	0.5	0.0528	2.901	3.2484	11.9765
270.28	110.55	-3.077	0.5	0.0528	2.851	3.1719	11.2563
270.35	110.92	-3.262	0.5	0.0528	2.853	3.154	10.5486
327.54	92.9	20.004	0.5	0.0528	4.923	5.0678	2.9413
329.1	91.24	9.793	0.5	0.0528	4.179	4.3058	3.0353
329.81	93.25	5.005	0.5	0.0528	3.925	4.0261	2.5766
330.2	95.4	4.079	0.5	0.0528	3.89	3.9803	2.3223
329.94	96.37	3.249	0.5	0.0528	3.872	3.9446	1.8744
330.94	94.3	-0.396	0.5	0.0528	3.424	4.2022	22.7274
222.07	93.49	19.675	0.5	0.0531	4.705	4.5367	-3.5767
221.06	93.09	9.907	0.5	0.0531	3.837	3.8659	0.7528
220.89	93.79	4.666	0.5	0.0531	3.502	3.5984	2.7532
220.22	94.06	0.058	0.5	0.0531	3.266	3.5179	7.7137
220.6	94.4	-0.129	0.5	0.0531	3.248	3.2435	-0.1383
220.17	94.86	-3.691	0.5	0.0531	2.598	2.7666	6.4903
271.35	111.84	20.297	0.5	0.0531	5.043	4.8499	-3.8297
271.07	78.32	20.188	0.5	0.0531	5.098	4.8922	-4.0371
271.56	93.87	20.172	0.5	0.0531	5.078	4.8692	-4.1127
270.32	110.39	19.992	0.5	0.0531	4.982	4.8228	-3.1955
269.6	78.51	19.886	0.5	0.0531	5.045	4.8602	-3.6633
271.56	94.28	19.652	0.5	0.0531	4.994	4.828	-3.3246
270.66	77.79	10.161	0.5	0.0531	4.172	4.1701	-0.045
271.07	111.59	9.878	0.5	0.0531	4.075	4.0842	0.2246
270.9	93.64	9.863	0.5	0.0531	4.155	4.1203	-0.8362
271.53	77.99	5.179	0.5	0.0531	3.823	3.9004	2.0257
271.42	94.25	4.81	0.5	0.0531	3.765	3.845	2.1258
270.73	111.02	4.542	0.5	0.0531	3.728	3.7908	1.6843
272.69	78.51	2.079	0.5	0.0531	3.597	3.7975	5.5752
271.52	111.6	1.17	0.5	0.0531	3.568	3.6946	3.5472
270.32	112.17	0.896	0.5	0.0531	3.532	3.6873	4.3965
270.52	78.99	0.754	0.5	0.0531	3.48	3.7726	8.4089
269.93	111.86	0.474	0.5	0.0531	3.543	3.6881	4.0942
271.84	92.52	0.453	0.5	0.0531	3.558	3.746	5.2833
270.59	112.41	0.155	0.5	0.0531	3.302	3.6964	11.9451
272.23	77.58	-0.634	0.5	0.0531	3.208	3.7034	15.442
270.77	93.6	-2.303	0.5	0.0531	3.06	3.2603	6.5447
270.96	111.25	-2.743	0.5	0.0531	3.009	3.2116	6.7326
329.43	92.7	19.979	0.5	0.0531	5.426	5.1349	-5.3652
329.74	93.22	10.084	0.5	0.0531	4.462	4.3767	-1.9109
330.29	93.7	5.638	0.5	0.0531	4.112	4.1086	-0.0831
330.21	93.41	1.977	0.5	0.0531	3.917	3.9657	1.2423
330.66	94.48	0.557	0.5	0.0531	3.771	3.9479	4.6906
329.4	94.04	-1.72	0.5	0.0531	3.4	3.7315	9.7512
222.06	94.27	20.632	0.5	0.0676	7.491	7.6362	1.9384
221.49	91.26	10.381	0.5	0.0676	6.579	6.5714	-0.1157
222.12	94.98	4.796	0.5	0.0676	6.318	6.1516	-2.6341
221.78	93.57	1.886	0.5	0.0676	6.127	6.0375	-1.46
222.4	94.75	-1.573	0.5	0.0676	4.59	4.7675	3.8665
220.88	94.32	-1.972	0.5	0.0676	4.494	4.565	1.5803
272.31	92.98	20.238	0.5	0.0676	7.91	8.1078	2.5009
271.12	93.22	19.974	0.5	0.0676	7.874	8.0642	2.4154
270.31	111.83	19.856	0.5	0.0676	7.857	7.9967	1.7785
270.48	91.87	19.61	0.5	0.0676	7.821	8.0181	2.5195

269.99	110.55	19.466	0.5	0.0676	7.813	7.9488	1.7376
270.91	111.71	9.669	0.5	0.0676	6.806	6.8878	1.2015
269.48	94.03	9.4	0.5	0.0676	6.771	6.9092	2.0409
272.18	94.4	5.407	0.5	0.0676	6.552	6.6147	0.9568
270.74	111.65	2.876	0.5	0.0676	6.481	6.4047	-1.178
271.48	112.65	2.67	0.5	0.0676	6.406	6.3976	-0.1311
271.83	96.16	2.562	0.5	0.0676	6.361	6.4592	1.5438
272.68	112.03	1.57	0.5	0.0676	6.411	6.3791	-0.498
271.33	97.82	1.518	0.5	0.0676	6.326	6.423	1.5341
271.59	98.74	1.294	0.5	0.0676	6.247	6.419	2.754
270.38	111.58	1.061	0.5	0.0676	6.355	6.3594	0.0685
270.22	113.19	0.596	0.5	0.0676	6.355	6.3551	0.0013
270.88	93.93	-0.179	0.5	0.0676	5.321	6.4219	20.689
271.02	112.58	-1.844	0.5	0.0676	4.982	5.1001	2.3709
329.54	98.48	20.036	0.5	0.0676	8.394	8.5415	1.757
329.93	98.72	19.961	0.5	0.0676	8.398	8.5333	1.6112
329.83	100.26	9.968	0.5	0.0676	7.282	7.3769	1.3032
330.39	102.75	5.109	0.5	0.0676	6.92	6.9554	0.5109
328.22	103.09	4.266	0.5	0.0676	6.837	6.8868	0.7287
329.69	105.19	2.051	0.5	0.0676	5.84	6.7834	16.1549
329.81	107.54	2.006	0.5	0.0676	6.687	6.7729	1.2852
327.38	106.31	1.918	0.5	0.0676	6.618	6.7611	2.1623
330.96	104.66	1.838	0.5	0.0676	6.508	6.7867	4.2819
220.93	92.3	20.029	0.5	0.0763	9.79	9.7529	-0.3785
220.54	94.79	9.785	0.5	0.0763	9.083	8.4566	-6.8966
221.07	99.66	4.53	0.5	0.0763	8.759	7.9944	-8.7289
221.35	101.46	1.394	0.5	0.0763	7.882	7.8712	-0.1365
222.09	101.85	1.354	0.5	0.0763	8.024	7.8786	-1.8126
222.07	100.89	1.333	0.5	0.0763	7.854	7.8817	0.3532
222.13	102.83	1.212	0.5	0.0763	8.219	7.874	-4.1978
221.15	93.8	-0.275	0.5	0.0763	6.362	7.212	13.3612
271.07	102.39	19.673	0.5	0.0763	10.357	10.3402	-0.1618
270.62	102.44	19.054	0.5	0.0763	10.256	10.2428	-0.129
270.29	105.5	9.64	0.5	0.0763	9.099	8.9903	-1.1946
272.16	109.72	5.29	0.5	0.0763	8.876	8.5758	-3.3824
271.1	109.38	4.786	0.5	0.0763	8.852	8.5282	-3.6583
271.2	106.44	1.87	0.5	0.0763	7.108	8.3979	18.1466
272.53	114.18	1.591	0.5	0.0763	8.3	8.3678	0.8174
271.35	112.51	1.452	0.5	0.0763	8.086	8.3615	3.4068
272.14	114.67	1.326	0.5	0.0763	8.442	8.3584	-0.9901
329	116.27	19.446	0.5	0.0763	11.072	10.88	-1.7344
329.34	118.49	10.136	0.5	0.0763	9.666	9.5521	-1.1782
327.86	118.4	9.281	0.5	0.0763	9.596	9.4381	-1.6452
329.48	126.24	5.112	0.5	0.0763	9.185	8.9907	-2.1153
330.53	127.21	2.405	0.5	0.0763	7.666	8.8192	15.0428
329.91	134.97	2.048	0.5	0.0763	8.848	8.7603	-0.9907
330.01	132.39	2.021	0.5	0.0763	8.903	8.7737	-1.4518
328.56	131.48	-0.363	0.5	0.0763	7.231	8.2044	13.4609
271.88	94.79	20.135	0.75	0.0435	3.148	3.0789	-2.1959
270.45	93.7	10.054	0.75	0.0435	2.496	2.4921	-0.157
271.45	93.88	2.412	0.75	0.0435	2.194	2.1535	-1.8447
270.89	93.91	1.435	0.75	0.0435	2.18	2.1284	-2.369
270.12	94.19	19.279	0.75	0.0528	4.603	4.4558	-3.1974
270.89	92.46	19.26	0.75	0.0528	4.539	4.4606	-1.7277
270.94	92.51	11.151	0.75	0.0528	3.838	3.777	-1.5903
269.99	92.97	10.464	0.75	0.0528	3.745	3.7185	-0.7078

271.16	92.68	9.604	0.75	0.0528	3.7	3.6569	-1.1651
270.93	93.25	2.401	0.75	0.0528	3.264	3.206	-1.7784
271.9	93.55	0.269	0.75	0.0528	3.206	3.1652	-1.2734
271.25	94.23	20.182	0.75	0.0676	7.697	7.4787	-2.8364
271.07	93.15	10.31	0.75	0.0676	6.322	6.1591	-2.5775
270.13	92.75	9.447	0.75	0.0676	6.204	6.0506	-2.4728
270.42	95.38	2.08	0.75	0.0676	5.649	5.3521	-5.2562
271.58	96.29	1.354	0.75	0.0676	5.591	5.3231	-4.7908
271.67	96.61	1.198	0.75	0.0676	5.567	5.318	-4.4735
270	97.41	1.103	0.75	0.0676	5.557	5.3028	-4.5746
271.18	100.98	20.084	0.75	0.0762	9.656	9.5063	-1.5498
270.25	97.03	9.5	0.75	0.0762	7.791	7.7567	-0.4406
270.79	97.72	2.667	0.75	0.0762	6.453	6.9465	7.6468
271.24	103.31	2.273	0.75	0.0762	7.092	6.8889	-2.8631
272.02	105.77	2.145	0.75	0.0762	7.024	6.8725	-2.1569
272.02	106.76	2.052	0.75	0.0762	6.856	6.8609	0.0708
271.93	93.07	20.35	1	0.0431	2.883	3.0446	5.6057
270.68	92.33	19.826	1	0.0431	2.816	3.0103	6.8992
272.01	92.66	9.961	1	0.0431	2.215	2.4432	10.3016
271.41	93.99	1.711	1	0.0431	1.942	2.0759	6.8961
271.62	93.31	20.105	1	0.0535	4.503	4.6462	3.1797
271.5	93.21	20.026	1	0.0528	4.517	4.5188	0.0399
271.25	94.01	19.543	1	0.0535	4.996	4.5914	-8.0987
271.07	92.51	10.165	1	0.0535	3.529	3.7636	6.6491
270.38	93.55	9.887	1	0.0535	4.002	3.7357	-6.6538
271.76	93.66	2.512	1	0.0535	3.42	3.2323	-5.4893
271.54	94.79	2.05	1	0.0535	2.96	3.2086	8.3985
269.74	94.15	1.258	1	0.0535	3.332	3.1784	-4.6108
271.38	94.53	0.962	1	0.0535	3.293	3.1746	-3.5941
271.18	95.3	20.574	1	0.0676	8.132	7.4473	-8.4203
271.11	94.14	9.789	1	0.0676	6.288	5.9392	-5.5468
271.08	94.35	2.257	1	0.0676	5.069	5.1455	1.5085
271.32	96.32	2.111	1	0.0676	5.47	5.1279	-6.2542
270.38	97.07	1.065	1	0.0676	5.297	5.0708	-4.2699
270.93	99.22	19.462	1	0.0762	9.472	9.2277	-2.5792
270.93	99.22	19.462	1	0.0762	9.472	9.2277	-2.5792
271.09	95.29	10.231	1	0.0762	7.654	7.613	-0.5359
270.93	98.76	2.867	1	0.0762	6.69	6.5813	-1.6244
271.56	101.22	2.414	1	0.0762	6.666	6.5292	-2.0524

A2: Pure R32/125 (50%/ 50%) by mass

Pup	Pdown	Tsub	L	D	Mact	Mcalc	% Diff
310.44	132.02	20.434	0.5	0.0432	3.444	3.358635	-2.47867
309.36	134.77	10.062	0.5	0.0432	2.668	2.709058	1.538913
309.78	131.99	5.629	0.5	0.0432	2.476	2.469837	-0.24892
309.73	135.82	2.246	0.5	0.0432	2.384	2.342438	-1.74338
309.65	129.13	-1.735	0.5	0.0432	2.318	2.112346	-8.87205
379.72	155.77	20.133	0.5	0.0432	3.63	3.587644	-1.16683
378.83	110.02	19.91	0.5	0.0432	3.644	3.530904	-3.10363
380.39	133.36	19.59	0.5	0.0432	3.564	3.534278	-0.83395
379.31	133.27	10.17	0.5	0.0432	2.914	2.928121	0.484588

379.57	156.22	9.962	0.5	0.0432	2.916	2.943303	0.936329
379.06	111.19	9.911	0.5	0.0432	2.949	2.886071	-2.13391
379.65	132	5.348	0.5	0.0432	2.7	2.668467	-1.16788
380.13	134.55	1.559	0.5	0.0432	2.544	2.538887	-0.20096
379.61	157.89	1.185	0.5	0.0432	2.559	2.565479	0.253169
378.8	112.71	1.01	0.5	0.0432	2.533	2.494349	-1.52591
379.33	133.87	-5.692	0.5	0.0432	2.055	1.986915	-3.31314
460.15	132.94	20.162	0.5	0.0432	3.889	3.789406	-2.56091
460.56	133.47	9.756	0.5	0.0432	3.221	3.110816	-3.42081
461.08	133	5.227	0.5	0.0432	2.929	2.869756	-2.02266
460.32	131.72	2.272	0.5	0.0432	2.785	2.754733	-1.08678
460.61	131.73	-2.249	0.5	0.0432	2.812	2.482679	-11.7113
309.36	133.67	20.067	0.5	0.0528	4.959	5.070886	2.256231
309.44	132.4	9.804	0.5	0.0528	4.075	4.123073	1.179703
310.38	134.07	4.643	0.5	0.0528	3.731	3.732589	0.042601
310.39	134	1.364	0.5	0.0528	3.61	3.567817	-1.16852
309.67	134.24	0.864	0.5	0.0528	3.542	3.553918	0.336469
308.98	133.39	-3.714	0.5	0.0528	2.941	2.956285	0.519708
380.51	115.71	20.108	0.5	0.0528	5.333	5.411588	1.473614
379.95	156.88	20.008	0.5	0.0528	5.306	5.451177	2.736087
379.6	132.48	19.776	0.5	0.0528	5.313	5.396154	1.565099
379.72	156.11	10.123	0.5	0.0528	4.434	4.520349	1.947431
379.76	117.78	9.888	0.5	0.0528	4.45	4.434929	-0.33867
379.03	132.3	9.664	0.5	0.0528	4.424	4.43707	0.295436
379.42	133.69	4.662	0.5	0.0528	4.139	4.05335	-2.06934
379.65	123.77	1.879	0.5	0.0528	3.977	3.884434	-2.32755
379.69	133.01	1.755	0.5	0.0528	4.047	3.899814	-3.63691
380.2	156.16	1.735	0.5	0.0528	3.982	3.950208	-0.79838
379.65	131.97	-0.205	0.5	0.0528	3.778	3.684507	-2.47466
461.06	132.28	20.249	0.5	0.0528	5.643	5.7826	2.473869
460.42	134.1	9.406	0.5	0.0528	4.722	4.734656	0.268018
461.12	138.35	5.326	0.5	0.0528	4.51	4.422825	-1.93294
460	139.25	4.712	0.5	0.0528	4.461	4.378474	-1.84994
461.13	146.99	1.932	0.5	0.0528	4.319	4.251782	-1.55634
461.13	142.8	-1.111	0.5	0.0528	4.258	3.959133	-7.01895
309.43	132.68	20.184	0.5	0.0674	8.416	8.610179	2.307257
310.31	133.32	10.364	0.5	0.0674	7.154	7.209345	0.773625
310.06	133.46	4.624	0.5	0.0674	6.682	6.518471	-2.44731
309.11	135.01	1.513	0.5	0.0674	6.453	6.267879	-2.86877
309.27	133.11	1.468	0.5	0.0674	6.445	6.261112	-2.85318
309.26	132.87	-1.52	0.5	0.0674	5.426	5.537805	2.060549
379.25	140.12	19.742	0.5	0.0674	8.952	9.168242	2.415576
379.84	144.36	10.078	0.5	0.0674	7.753	7.76593	0.166768
379.75	147.46	4.961	0.5	0.0674	7.317	7.152936	-2.24224
379.53	153.16	2.037	0.5	0.0674	7.083	6.920342	-2.29645
379.78	155.32	1.398	0.5	0.0674	6.998	6.894781	-1.47498
380.01	152.58	-0.701	0.5	0.0674	6.845	6.239181	-8.85053
460.65	149.1	19.481	0.5	0.0674	9.58	9.734323	1.610885
460.24	157.32	9.907	0.5	0.0674	8.373	8.324651	-0.57743
460.18	155.98	4.908	0.5	0.0674	7.921	7.712995	-2.62599
461.18	169.8	2.026	0.5	0.0674	7.626	7.519496	-1.39659

461.48	164.82	1.94	0.5	0.0674	7.57	7.499009	-0.93779
460.87	167.65	-1.867	0.5	0.0674	7.233	6.63006	-8.33596
310.35	133.73	20.165	0.5	0.0763	11.329	11.36361	0.30548
309.73	132.94	10.488	0.5	0.0763	9.556	9.648284	0.965719
310.18	135.77	5.131	0.5	0.0763	8.876	8.869722	-0.07073
310.1	141.17	1.833	0.5	0.0763	8.528	8.549576	0.253007
310.17	145.07	1.364	0.5	0.0763	8.2	8.534385	4.077862
310.08	140	-1.377	0.5	0.0763	6.899	7.500221	8.71461
309.94	141.71	-1.943	0.5	0.0763	6.742	7.398134	9.732037
380.4	150.17	19.969	0.5	0.0763	12.17	12.18455	0.119545
380.17	159.66	10.116	0.5	0.0763	10.409	10.44318	0.328414
380.24	150.56	5.231	0.5	0.0763	9.807	9.691262	-1.18016
380.71	158.35	1.594	0.5	0.0763	9.474	9.360815	-1.19469
380.69	157.3	1.569	0.5	0.0763	9.455	9.353321	-1.0754
381.6	159.05	1.38	0.5	0.0763	9.265	9.358833	1.012768
380.36	159.5	1.313	0.5	0.0763	9.202	9.345735	1.561998
379.86	153.93	-0.395	0.5	0.0763	7.977	8.662744	8.596511
459.78	161.29	19.423	0.5	0.0763	12.878	12.87925	0.00971
459.75	168.84	9.745	0.5	0.0763	11.186	11.14249	-0.389
461.3	168.98	5.083	0.5	0.0763	10.567	10.46849	-0.93227
460.38	177.19	2.039	0.5	0.0763	10.099	10.17637	0.76608
461.05	179.52	1.901	0.5	0.0763	10.076	10.18054	1.037547
460.5	177.05	-0.921	0.5	0.0763	9.277	9.273064	-0.04243
379.32	132	20.258	0.75	0.0528	5.265	5.271819	0.129507
379.52	133.1	9.939	0.75	0.0528	4.183	4.290924	2.580067
378.93	134.11	1.262	0.75	0.0528	3.607	3.735	3.548649
378.92	131.65	-3.766	0.75	0.0528	3.176	3.106081	-2.20148
379.25	133.16	19.909	0.751	0.0431	3.698	3.458644	-6.47257
379.66	133.76	9.799	0.751	0.0431	2.893	2.829579	-2.19221
379.23	134.08	1.56	0.751	0.0431	2.432	2.488453	2.321246
379.49	133.98	1.525	0.751	0.0431	2.47	2.488502	0.749089
379.63	132	-5.512	0.751	0.0431	2.1	1.956836	-6.81734
378.95	133	19.679	0.751	0.0676	8.591	8.640098	0.571501
378.83	136.48	9.713	0.751	0.0676	7.06	7.075445	0.218772
380.15	161.21	1.666	0.751	0.0676	6.331	6.265432	-1.03567
379.2	166.6	1.543	0.751	0.0676	6.286	6.271201	-0.23542
379.15	169.46	1.406	0.751	0.0676	6.239	6.27571	0.588402
378.99	167.92	1.373	0.751	0.0676	6.227	6.267333	0.647713
379.96	153.32	-1.231	0.751	0.0676	5.582	5.710685	2.305355
379.03	146.03	19.94	0.751	0.0762	11.011	11.13272	1.105404
378.83	149.7	9.543	0.751	0.0762	9.04	9.061369	0.236378
379.82	165.15	1.587	0.751	0.0762	8.15	7.995942	-1.89028
380.02	168.21	1.38	0.751	0.0762	8.08	7.998916	-1.00351
380.51	167.92	1.262	0.751	0.0762	8.121	7.995304	-1.54779
380.13	159.96	-0.609	0.751	0.0762	7.492	7.511221	0.256551
379.36	160.52	-1.565	0.751	0.0762	7.208	7.161986	-0.63838
379.39	136.04	20.028	0.998	0.06894	9.684	8.949701	-7.5826
379.72	140.03	19.851	0.998	0.06894	9.671	8.931384	-7.64777
379.49	140.82	10.092	0.998	0.06894	7.783	7.355116	-5.49767
380.62	140.68	9.762	0.998	0.06894	7.748	7.314617	-5.59348
379.59	136.75	9.592	0.998	0.06894	7.735	7.269676	-6.01583

378.86	149.95	1.744	0.998	0.06894	6.721	6.444114	-4.11972
380.15	152.34	1.426	0.998	0.06894	6.693	6.449137	-3.64356
379.64	154.15	1.36	0.998	0.06894	6.663	6.450304	-3.1922
379.15	146.48	-0.047	0.998	0.0676	6.129	6.065846	-1.03041
378.98	146.8	-0.5	0.998	0.0676	6.134	5.863994	-4.40179
380.27	147.12	-0.881	0.998	0.0676	5.911	5.731254	-3.04087
379.71	132.62	20.125	1	0.0431	3.034	3.428074	12.98859
379.85	133.64	9.833	1	0.0431	2.35	2.798861	19.10048
379.5	131.9	4.31	1	0.0431	2.195	2.543335	15.8695
380.06	134.34	2.121	1	0.0431	2.03	2.490787	22.69889
379.41	132.78	-6.136	1	0.0431	1.73	1.897159	9.662343
379.27	132.34	-8.717	1	0.0431	1.726	1.754912	1.675099
379.11	134.53	19.798	1	0.0528	5.077	5.161225	1.658945
379.06	133.52	9.591	1	0.0528	3.978	4.211765	5.876443
378.92	130.66	1.798	1	0.0528	3.437	3.727512	8.45248
379.17	136.45	1.383	1	0.0528	3.413	3.733632	9.394438
379.4	131.78	-2.361	1	0.0528	3.142	3.26121	3.794091
379.52	133.12	-4.028	1	0.0528	3.047	3.033776	-0.43399
379.3	145.48	19.988	1	0.0762	11.004	10.99799	-0.05463
379.17	151.01	9.693	1	0.0762	8.756	8.982799	2.590208
379.98	164.42	1.713	1	0.0762	7.67	7.95563	3.723988
379.02	164.2	1.661	1	0.0762	7.664	7.943449	3.646257
380.48	168.97	1.174	1	0.0762	7.596	7.955277	4.729817
378.94	161.25	-0.2	1	0.0762	7.303	7.568625	3.637202
379.23	161.85	-0.69	1	0.0762	7.011	7.396483	5.498257

A3: 1.0% Oil and R32/125/134a (23%/ 25%/ 52%) by mass

PUP	PDOWN	TSUB	L	D	MACT	MCALC	%DIFF
220.83	91.32	20.32	0.5	0.0528	4.372	4.3933	0.4862
221.55	92.72	9.871	0.5	0.0528	3.554	3.7013	4.1454
220.94	94.7	4.577	0.5	0.0528	3.417	3.4577	1.19
220.8	92.75	3.151	0.5	0.0528	3.41	3.4271	0.5015
220.88	93.04	2.751	0.5	0.0528	3.375	3.4195	1.3173
220.64	92.65	-3.647	0.5	0.0528	2.457	2.9048	18.2248
270.47	94.5	19.755	0.5	0.0528	4.597	4.6107	0.297
270.79	94.46	9.991	0.5	0.0528	3.86	3.9154	1.4341
271.45	95.97	4.812	0.5	0.0528	3.555	3.6495	2.6573
271.49	97.36	2.834	0.5	0.0528	3.53	3.5857	1.5778
272.2	96.29	-2.563	0.5	0.0528	2.891	3.3481	15.8095
271.12	96.38	-2.752	0.5	0.0528	2.846	3.2965	15.8286
329.58	94.23	20.414	0.5	0.0528	4.982	4.9166	-1.3119
329.12	92.42	10.114	0.5	0.0528	4.188	4.122	-1.5759
329.07	93.58	5.001	0.5	0.0528	3.91	3.828	-2.0974
329.86	95.17	3.631	0.5	0.0528	3.931	3.7695	-4.1085
328.84	94.88	2.848	0.5	0.0528	3.706	3.7453	1.0596
329.01	92.94	-2.706	0.5	0.0528	3.153	3.6931	17.1283
220.52	92.56	19.657	0.5	0.0676	7.316	7.3588	0.5855
221.21	94.37	9.922	0.5	0.0676	6.604	6.4507	-2.3214

221.76	95.61	5.804	0.5	0.0676	6.467	6.201	-4.1138
221.27	95.52	5.192	0.5	0.0676	6.447	6.1716	-4.272
220.49	98.37	2.503	0.5	0.0676	6.21	6.089	-1.9483
221.35	100.31	2.109	0.5	0.0676	6.195	6.0861	-1.7574
221.9	93.7	-2.225	0.5	0.0676	5.304	4.9459	-6.7506
270.72	100.91	20.115	0.5	0.0676	7.76	7.8627	1.3231
271.73	102.32	10.375	0.5	0.0676	6.667	6.8607	2.9055
270.6	104.9	4.638	0.5	0.0676	6.338	6.4659	2.0174
270.54	108.56	2.568	0.5	0.0676	6.223	6.3881	2.6533
270.8	105.62	-2.289	0.5	0.0676	5.976	5.3547	-10.3961
272.55	105.04	-2.291	0.5	0.0676	5.928	5.3713	-9.391
329.24	104.28	20.052	0.5	0.0676	8.263	8.2906	0.3344
329.49	106.68	10.091	0.5	0.0676	7.161	7.178	0.2377
328.42	111.54	4.926	0.5	0.0676	6.785	6.7643	-0.3047
329.45	112.37	4.879	0.5	0.0676	6.778	6.7629	-0.2233
330.16	117.72	3.103	0.5	0.0676	6.586	6.6603	1.1282
329.94	113.7	-2.803	0.5	0.0676	5.922	5.7471	-2.9539

A4: 2.15% Oil and R32/125/134a

Pup	Pdown	Tsub	Length	Diameter	Mdotact	Mdotcalc	%Diff
380.62	132.32	20.226	0.5	0.0432	3.689	3.536306	-4.13918
379.34	132.79	9.78	0.5	0.0432	2.889	2.88945	0.01556
380.01	132.45	5.044	0.5	0.0432	2.673	2.632653	-1.50943
379.55	132.44	1.966	0.5	0.0432	2.588	2.492717	-3.68173
379.98	132.08	1.709	0.5	0.0432	2.541	2.483187	-2.2752
379.12	133.18	0.971	0.5	0.0432	2.499	2.457419	-1.66392
379.1	133.77	-2.546	0.5	0.0432	2.214	2.166751	-2.13412
379.81	132.89	-2.866	0.5	0.0432	2.217	2.174384	-1.92223
310.73	133.63	20.206	0.5	0.0528	5.02	5.087245	1.33954
309.72	134.25	19.825	0.5	0.0528	4.984	5.049347	1.311135
310.23	133.94	10.287	0.5	0.0528	4.073	4.160596	2.150645
309.74	133.49	9.868	0.5	0.0528	4.073	4.119206	1.134441
309.76	131.93	5.247	0.5	0.0528	3.734	3.710186	-0.63776
309.94	131.67	4.834	0.5	0.0528	3.709	3.675372	-0.90666
309.23	133.76	0.822	0.5	0.0528	3.461	3.385429	-2.18351
309.4	135.55	0.686	0.5	0.0528	3.444	3.385323	-1.70375
309.46	132.38	-2.18	0.5	0.0528	3.069	2.946352	-3.99636
309.67	132.64	-3.428	0.5	0.0528	2.927	2.868348	-2.00384
379.53	134.67	19.843	0.5	0.0528	5.318	5.295735	-0.41866
379.07	136.12	9.621	0.5	0.0528	4.409	4.39289	-0.3654
379.63	132.23	5.008	0.5	0.0528	4.094	4.027935	-1.61369
380.08	134.56	1.584	0.5	0.0528	3.973	3.830509	-3.58649
379.62	135.26	1.079	0.5	0.0528	3.906	3.80775	-2.51536
380.07	133.59	-1.886	0.5	0.0528	3.431	3.328881	-2.97637
379.97	133.38	-3.338	0.5	0.0528	3.305	3.250963	-1.63501
459.86	132.92	20.037	0.5	0.0528	4.752	5.517195	16.10259
461.61	133.84	10.602	0.5	0.0528	4.805	4.733553	-1.48694

461.02	132.83	4.93	0.5	0.0528	4.461	4.353018	-2.42059
461.34	133.97	2.141	0.5	0.0528	4.262	4.225008	-0.86795
460.89	133.29	-1.8	0.5	0.0528	3.693	3.765162	1.95402
460.82	131.65	-3.241	0.5	0.0528	3.623	3.656689	0.92987
309.59	131.84	19.654	0.5	0.0674	8.35	8.439376	1.070372
310.35	134.05	10.019	0.5	0.0674	6.94	7.101657	2.329347
310.14	133.79	9.858	0.5	0.0674	6.947	7.077945	1.884916
310.51	133.85	5.188	0.5	0.0674	6.506	6.491887	-0.21693
309.29	133.83	1.146	0.5	0.0674	6.211	6.05701	-2.47931
310.71	133.48	1.12	0.5	0.0674	6.185	6.066806	-1.91098
310.27	134.87	-0.445	0.5	0.0674	5.389	5.308304	-1.49742
309.62	133.92	-1.511	0.5	0.0674	5.14	5.213445	1.428883
378.96	143.4	20.085	0.5	0.0674	9.005	8.97342	-0.35069
379.47	139.44	9.939	0.5	0.0674	7.645	7.617182	-0.36387
379.54	142.59	5.064	0.5	0.0674	7.184	7.102042	-1.14085
379.27	147.31	1.322	0.5	0.0674	6.838	6.824261	-0.20092
380.42	147.15	1.186	0.5	0.0674	6.788	6.825299	0.549479
380.09	147.96	1.13	0.5	0.0674	6.798	6.824439	0.388925
379.99	144.03	-1.07	0.5	0.0674	5.726	5.84425	2.065146
379.65	143.02	-1.906	0.5	0.0674	5.59	5.710267	2.151469
460.71	156.31	19.653	0.5	0.0674	9.695	9.35576	-3.49912
460.8	147.51	9.716	0.5	0.0674	8.313	8.116024	-2.3695
460.1	151.23	4.946	0.5	0.0674	7.882	7.705054	-2.24494
461.3	156.21	1.842	0.5	0.0674	7.464	7.554937	1.21834
460.86	157.01	1.811	0.5	0.0674	7.376	7.555868	2.43856
460.66	159.12	-0.2	0.5	0.0674	6.434	6.779874	5.375721
460.51	152.92	-0.805	0.5	0.0674	6.248	6.647975	6.401646
379.1	153.02	19.618	0.5	0.0763	12.057	11.75769	-2.48247
379.17	160.27	9.784	0.5	0.0763	10.225	10.26705	0.411217
379.77	166.98	4.98	0.5	0.0763	9.6	9.723675	1.28828
379.18	178.52	1.03	0.5	0.0763	8.952	9.46226	5.69995
379.94	170.34	-0.5	0.5	0.0763	8.162	7.988684	-2.12345
380.19	170.5	-0.6	0.5	0.0763	8.151	7.956423	-2.38715
379.96	132.22	20.101	0.75	0.0528	5.253	5.265684	0.241457
379.72	132.39	9.989	0.75	0.0528	4.13	4.31501	4.479653
379.93	134.75	1.809	0.75	0.0528	3.616	3.684364	1.890598
379.41	135.34	1.175	0.75	0.0528	3.586	3.648284	1.736867
380.07	134.45	-2.491	0.75	0.0528	3.233	3.289741	1.755071
380.08	134.44	-3.921	0.75	0.0528	3.16	3.23016	2.220265
379.19	132.95	19.782	0.751	0.0676	8.685	8.537644	-1.69667
379.54	133.36	9.979	0.751	0.0676	7.036	7.049685	0.194497
379.77	141.68	1.902	0.751	0.0676	6.264	6.097859	-2.65232
379.1	141.53	-0.2	0.751	0.0676	5.919	5.531913	-6.53973
379.3	143.37	-0.3	0.751	0.0676	5.846	5.504198	-5.84676
379.66	132.77	19.587	1	0.0528	5.123	5.251021	2.498942
378.97	131.27	1.519	1	0.0528	3.372	3.65175	8.296271
377.62	133.59	1.453	1	0.0528	3.296	3.6514	10.78276
379.82	132.73	-0.25	1	0.0528	3.378	3.489089	3.288607
379.84	130.77	-0.35	1	0.0528	3.33	3.451509	3.648907
379.47	134.53	20	1	0.0676	9.143	8.631537	-5.59404
379.99	134.49	10.445	1	0.0676	7.244	7.159178	-1.17092

379.54	141.42	1.835	1	0.0676	6.127	6.088179	-0.6336
379.81	141.31	-0.16	1	0.0676	5.727	5.654951	-1.25807
379.47	140.07	-0.21	1	0.0676	5.713	5.688934	-0.42125

** When calculations are being made in the twophase region, the value of SUBC is set equal to zero.

APPENDIX B

QUALITY ASSURANCE AND UNCERTAINTY ANALYSIS

The original quality assurance plan outlined possible test conditions for the short tube orifice test facility. The actual test sequence and the methods of assuring data quality will be described below. All data quality objectives were met throughout the short tube orifice tests.

All tests were designed to reveal the effects of the main operating parameter on mass flowrate through a short tube orifice. Two R22 replacement refrigerants were tested under the same condensing and evaporating conditions. The ternary zeotropic refrigerant, AC9000, and the binary near-azeotropic refrigerant, AZ20, were tested to determine the mass flowrate through short tube orifices as a function of the primary variables upstream pressure, downstream pressure, upstream subcooling, orifice length, and orifice diameter. Tables B1 and B2 list the tests performed for the pure ternary refrigerant while Tables B4 and B5 list the tests performed for the pure binary refrigerant. Oil and refrigerant mixture testing was done within a limited range of the primary variables. The oil tests performed are shown in Tables B6 and B7.

The asterisk subscripts appearing in the upper portion of a table adjacent to a diameter and again in the lower portion of a table adjacent to a downstream pressure indicate that these were the only orifices tested at varying downstream pressures. It was unnecessary to test all orifices at varying downstream pressures due to the choked conditions of the tests. Downstream pressure was shown not to affect mass flowrate as long as the flow was choked, which was the case for all tests.

Short tube orifice length was tested at only one upstream pressure. Previous investigations have shown that testing at other upstream pressures was unnecessary due to the similarity of flow trends for the different lengths.

Table B1: Test Matrix for Pure AC9000 with Orifice Length of 0.5 in (12.7 mm)

Diameter, in (mm)		Length, in (mm)	
0.0431 (1.09)		0.500 (12.7)	
0.0528 (1.34) ****			
0.0676 (1.72)			
0.0763 (1.94) ****			
P_{up} psia (kPa)	**P_{down} psia (kPa)**	**T_{up} °F (°C)**	**T_{sub} °F (°C)**
221.06 (1524)	93.65 (646)	75 (23.9)	20 (11.1)
		85 (29.4)	10 (5.6)
		90 (32.2)	5 (2.8)
		95 (35)	0 (0)
		95 (35)	5%
271.25 (1870)	78.37 (540) ****	90 (32.2)	20 (11.1)
	93.65 (646)	100 (37.8)	10 (5.6)
	111.07 (765) ****	105 (40.6)	5 (2.8)
		110 (43.3)	0 (0)
		110 (43.3)	5%
329.31 (2271))	93.65 (646)	105 (40.6)	20 (11.1)
		115 (46.1)	10 (5.6)
		120 (48.9)	5 (2.8)
		125 (51.7)	0 (0)
		125 (51.7)	5%

Table B2: Test Matrix for Pure AC9000 with Orifice Lengths of 0.75 in (19.05 mm) and 1.00 in (25.4 mm)

Diameter, in (mm)		Length, in (mm)	
0.0431 (1.09)		0.750 (19.05) 1.000 (25.4)	
0.0528 (1.34)			
0.0676 (1.72)			
0.0763 (1.94)			
P_{up} psia (kPa)	**P_{down} psia (kPa)**	**T_{up} °F (°C)**	**T_{sub} °F (°C)**
271.25 (1870)	93.65 (646)	90 (32.2)	20 (11.1)
		100 (37.8)	10 (5.6)
		105 (40.6)	5 (2.8)
		110 (43.3)	0 (0)
		110 (43.3)	5%

Table B3: Test Matrix for Pure AZ20 with Orifices of Length 0.5 in (12.7 mm)

Diameter, in (mm)		Length, in (mm)	
0.0431 (1.09) ****		0.500 (12.7)	
0.0528 (1.34) ****			
0.0676 (1.72)			
0.0763 (1.94)			
P_{up} psia (kPa)	**P_{down} psia (kPa)**	**T_{up} °F (°C)**	**T_{sub} °F (°C)**
309.79 (2136)	132.71 (915)	75 (23.9)	20 (11.1)
		85 (29.4)	10 (5.6)
		90 (32.2)	5 (2.8)
		95 (35)	0 (0)
		95 (35)	5%
379.66 (2618)	111.51 (769) ****	90 (32.2)	20 (11.1)
	132.71 (915)	100 (37.8)	10 (5.6)
	156.89 (1082) ****	105 (40.6)	5 (2.8)
		110 (43.3)	0 (0)
		110 (43.3)	5%
460.66 (3176))	93.65 (646)	105 (40.6)	20 (11.1)
		115 (46.1)	10 (5.6)
		120 (48.9)	5 (2.8)
		125 (51.7)	0 (0)
		125 (51.7)	5%

Table B4: Test Matrix for Pure AZ20 with Orifices of Length 0.75 in (19.05 mm) and 1.00 in (25.4 mm)

Diameter, in (mm)		Length, in (mm)	
0.0431 (1.09)		0.750 (19.05) 1.000 (25.4)	
0.0528 (1.34)			
0.0676 (1.72)			
0.0763 (1.94)			
P_{up} psia (kPa)	**P_{down} psia (kPa)**	**T_{up} °F (°C)**	**T_{sub} °F (°C)**
379.66 (2618)	132.71 (915)	90 (32.2)	20 (11.1)
		100 (37.8)	10 (5.6)
		105 (40.6)	5 (2.8)
		110 (43.3)	0 (0)
		110 (43.3)	5%

Table B5: Oil Tests for AC9000

Diameter, in (mm)		Length, in (mm)	
0.0528 (1.34)		0.500 (12.7)	
0.0676 (1.72)			
P_{up} psia (kPa)	**P_{down} psia (kPa)**	**T_{up} °F (°C)**	**T_{sub} °F (°C)**
221.06 (1524)	93.65 (646)	75 (23.9)	20 (11.1)
		85 (29.4)	10 (5.6)
		90 (32.2)	5 (2.8)
		95 (35)	0 (0)
		95 (35)	5%
271.25 (1870)	93.65 (646)	90 (32.2)	20 (11.1)
		100 (37.8)	10 (5.6)
		105 (40.6)	5 (2.8)
		110 (43.3)	0 (0)
		110 (43.3)	5%
329.31 (2271))	93.65 (646)	105 (40.6)	20 (11.1)
		115 (46.1)	10 (5.6)
		120 (48.9)	5 (2.8)
		125 (51.7)	0 (0)
		125 (51.7)	5%

Table B6: Oil Tests for AZ20

Diameter, in (mm)		Length, in (mm)	
0.0431 (1.09) Middle Pressure Only		0.500 (12.7)	
0.0528 (1.34)		0.750 (19.05) Middle Pressure with 0.0528 (1.34) and 0.0676 (1.72) Only	
0.0676 (1.72)		1.00 (25.40) Middle Pressure with 0.0528 (1.34) and 0.0676 (1.72) Only	
0.0763 (1.94) Middle Pressure Only			
P_{up} psia (kPa)	**P_{down} psia (kPa)**	**T_{up} °F (°C)**	**T_{sub} °F (°C)**
309.79 (2136)	132.71 (915)	75 (23.9)	20 (11.1)
		85 (29.4)	10 (5.6)
		90 (32.2)	5 (2.8)
		95 (35)	0 (0)
		95 (35)	5%
379.66 (2618)	132.71 (915)	90 (32.2)	20 (11.1)
		100 (37.8)	10 (5.6)
		105 (40.6)	5 (2.8)
		110 (43.3)	0 (0)
		110 (43.3)	5%
460.66 (3176))	93.65 (646)	105 (40.6)	20 (11.1)
		115 (46.1)	10 (5.6)
		120 (48.9)	5 (2.8)
		125 (51.7)	0 (0)
		125 (51.7)	5%

Data Quality Objectives

The quality assurance plan was formed to specify the type of data necessary to formulate a flow model for short tube orifices and to quantify the acceptable error in any measurements undertaken during that effort. Before any tests were performed, all equipment was inspected and calibrated. During the process of generating data for the flow model, a quality assurance supervisor audited the test facility to determine if data quality goals were being met. Every effort was made to insure consistent and accurate measurement of the primary variables. Table B7 lists the variables necessary for the flow model in addition to the measurement method and associated error.

Table B7: Data Quality Summary for Directly Measured Variables

Measured Quantity	Measurement Method	Bias Error	Precision Error	Total Error	Acceptable Total Error
Pressure	Stainless Steel Diaphragm Pressure Transducer	0.1% of measured value	≈ 0.5 psia (3.4 kPa)	≈ 0.8 psia (5.5 kPa)	1 psia (6.9 kPa)
Temperature	Thermocouple T-type	0.2°F (0.36°C)	0.3°F (0.54°C)	0.5°F (0.90°C)	1.0°F (1.8°C)
Mass Flowrate	Coriolis Effect Mass Flow Meter	0.4% of measured flowrate	18 lbm / h (8.2 kg/h)	≈ 19.0 lbm / h (8.6 kg/h)	30 lbm / h (13.6 kg/h)
Length	Dial Calipers	0.0005 in (.012 mm)	.001 in (.025 mm)	0.0015 in (.038 mm)	0.002 in (.050 mm)
Diameter	Plug Gages	0.00001 in (.00025 mm)	0.0005 in (.012 mm)	0.00051 in (.013 mm)	0.001 in (.025 mm)
Heat Tape Power	Watt Transducer	0.5% of reading	Unknown	0.5% of reading	NA
Weight	Balance Beam Scale	.017 oz (0.5 g)	.035 oz (1.0 g)	.053 oz (1.5 g)	.035 oz (1.0g)

Pressure measurements were performed at various locations around the flow loop. During testing the upstream pressure had to be maintained within ±1 psia (6.9 kPa) of the desired value for the data to be acceptable. Any data that fell outside of this range was not

used to develop the flow model, but it was still included in the data comparison shown in Appendix A. The main reason for the upstream pressure criteria not always being met was the inability to match pump speed and bypass valve opening to produce the desired pressure. The diaphragm pump used to circulate the refrigerant consisted of three separate diaphragm cavities. If the pump speed were allowed to drop too low, the resulting flow pulsations would cause pressure to oscillate. To prevent these oscillations, the pump speed needed to remain high, with the main flow adjustment being initiated with the bypass valve.

Temperatures were controlled using the hot water and chilled water flow loops and their various bypass and control valves. At low mass flowrates, the temperature of the upstream refrigerant was easily maintained. As orifice diameter increased, increasing mass flowrate caused more variation in the upstream temperature. Upstream temperature control was also affected by upstream pressure control. Higher pressures caused higher flowrate which in turn lowered the upstream temperature. If the hot water flowrate was not adjusted accordingly, the upstream temperature could vary beyond the limit specified. Generally, any data that failed to meet temperature control criteria was discarded and the tests retaken.

Mass flowrate was measured with a coriollis effect mass flowmeter in the subcooled liquid line before the heat tape and orifice test section. Mass flowrate was the variable being modeled and therefore care was taken to assure accurate mass flow determination. Before testing with each refrigerant, the meter was calibrated using warm water. A bucket and stop watch method was used. Generally linear calibration produced agreement within 1% of the values supplied by the manufacturer. The main factor affecting steady flowrate was the pulsing nature of the three cavity pump. Pump rpm was kept high to maintain smooth flow through the flow meter.

An energy balance on the heat tape section of the flow loop revealed the expression used to calculate inlet quality:

$$x = \frac{Q_H - Q_L}{\dot{m} h_{fg}} + \frac{h_{in} - h_f}{h_{fg}}$$

where
- x = quality (mass vapor / total mass)
- Q_H = heat energy added, Btu/min (Watts)
- Q_L = heat energy lost through insulation, Btu/min (Watts)
- $\dot{m}$ = mass flowrate of refrigerant, lbm/ min (kg/h)
- h_{fg} = enthalpy of vaporization (h_g - h_f), Btu/lbm (kJ/kg)
- h_{in} = heat tape inlet refrigerant enthalpy, Btu/lbm (kJ/kg)
- h_f = enthalpy of saturated liquid, Btu/lbm (kJ/kg)
- h_g = enthalpy of saturated vapor, Btu/lbm (kJ/kg)

The propagation of error through the quality equation can be determined using the following equation:

$$\omega_x^2 = \left(\frac{\partial x}{\partial Q_H}\omega_{Q_H}\right)^2 + \left(\frac{\partial x}{\partial Q_L}\omega_{Q_L}\right)^2 + \left(\frac{\partial x}{\partial \dot{m}}\omega_{\dot{m}}\right)^2 + \left(\frac{\partial x}{\partial h_{in}}\omega_{h_{in}}\right)^2 + \left(\frac{\partial x}{\partial h_f}\omega_{h_f}\right)^2 + \left(\frac{\partial x}{\partial h_g}\omega_{hg}\right)^2$$

Using the equation for quality, the error propagation equation reduces to the following form:

$$\omega_x^2 = \left(\frac{\omega_{Q_H}}{\dot{m} h_{fg}}\right)^2 + \left(\frac{\omega_{Q_L}}{\dot{m} h_{fg}}\right)^2 + \left(\frac{\omega_{\dot{m}}(Q_H - Q_L)}{\dot{m}^2 h_{fg}}\right)^2 + \left(\frac{\omega_{h_{in}}}{h_{fg}}\right)^2 + \left(\frac{\omega_{h_f}\left(Q_H - Q_L + \dot{m}(h_{in} - h_f)\right)}{\dot{m} h^2{}_{fg}}\right)^2 +$$

$$\left(\frac{\omega_{h_g}\left(Q_H - Q_L + \dot{m}(h_{in} - h_f)\right)}{\dot{m} h^2{}_{fg}}\right)^2$$

$$C_o = \frac{M_{oil}}{M_r}$$

where M_{oil} = mass of oil, ounces (grams)

M_r = mass of refrigerant, ounces (grams)

Using this equation the propagation of error through the oil concentration equation could be calculated as follows:

$$\omega_o^2 = \left(\frac{\omega_{M_{oil}}}{M_r}\right)^2 + \left(\frac{M_{oil}\omega_r}{M_r^2}\right)^2$$

where ω_o = uncertainty in oil concentration

$\omega_{M_{oil}}$ = uncertainty in mass of oil, ounces (grams)

ω_r = uncertainty in mass of refrigerant, ounces (grams)

Uncertainties Calculated

The uncertainty in upstream quality and oil concentration were determined using actual test data. Table B9 and B10 gives examples of uncertainty for tests done with the ternary and binary refrigerants.

Table B9: Example Quality Uncertainty Values

	$\dot{m}$, lb/h (kg/h)	Q_H, Btu/min (Watts)	Q_L, Btu/min (Watts)	h_{in}, Btu/lbm (kJ/kg)	h_f, Btu/lbm (kJ/kg)	h_g, Btu/lbm (kJ/kg)	X	W_x	% Error
AC9000	119 (54)	4.15 (73)	0.82 (14)	45.36 (105.5)	46.63 (108.5)	122.02 (283.8)	0.981	0.007483	0.76
	275 (125)	13.88 (244)	1.98 (35)	45.40 (105.6)	46.68 (108.6)	122.03 (283.8)	1.573	0.003678	0.23
	269 (122)	13.86 (243)	1.98 (35)	45.36 (105.5)	46.63 (108.5)	122.02 (283.8)	1.972	0.003787	0.19
AZ20	139 (63)	4.82 (85)	0.90 (16)	41.77 (97.2)	43.97 (102.3)	119.24 (277.4)	1.735	0.006433	0.37
	123 (56)	12.89 (227)	1.87 (33)	49.50 (115.1)	50.92 (118.4)	119.25 (277.4)	5.692	0.013509	0.24
	169 (77)	3.91 (69)	0.79 (14)	57.13 (132.9)	58.82 (136.8)	118.77 (276.3)	2.249	0.006261	0.28